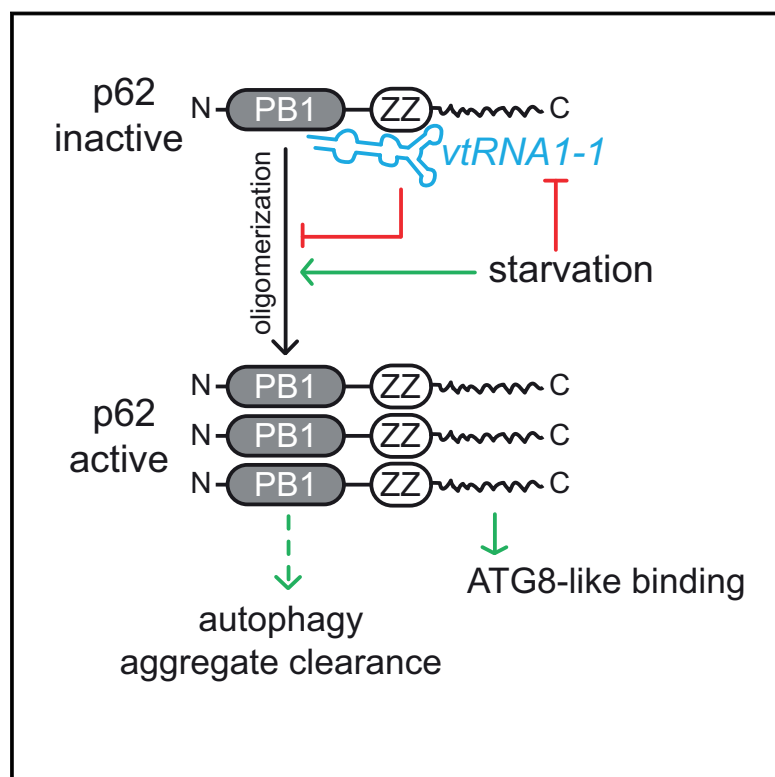


The Small Non-coding Vault RNA1-1 Acts as a Riboregulator of Autophagy

Graphical Abstract



Authors

Rastislav Horos, Magdalena Büscher, Rozemarijn Kleinendorst, ..., Wolfgang Huber, Carsten Sachse, Matthias W. Hentze

Correspondence

horos@embl.de (R.H.), hentze@embl.de (M.W.H.)

In Brief

A biological function of vault RNAs is to directly modulate the oligomerization state of p62, thereby controlling autophagy.

Highlights

- The selective human autophagy receptor p62/sequestosome-1 is an RNA-binding protein
- p62 engages the small non-coding vault RNA1-1 as a major interacting RNA
- Vault RNA1-1 riboregulates p62-dependent autophagy and aggregate clearance
- Mechanistically, vault RNA1-1 interferes with p62 multimerization



The Small Non-coding Vault RNA1-1 Acts as a Riboregulator of Autophagy

Rastislav Horos,^{1,5,*} Magdalena Büscher,^{1,4,5} Rozemarijn Kleinendorst,¹ Anne-Marie Alleaume,¹ Abul K. Tarafder,¹ Thomas Schwarzl,¹ Dmytro Dziuba,¹ Christian Tischer,¹ Elisabeth M. Zielonka,¹ Asli Adak,¹ Alfredo Castello,² Wolfgang Huber,¹ Carsten Sachse,^{1,3} and Matthias W. Hentze^{1,6,*}

¹European Molecular Biology Laboratory, Meyerhofstrasse 1, 69117 Heidelberg, Germany

²Department of Biochemistry, University of Oxford, South Parks Road, Oxford OX1 3QU, UK

³Ernst Ruska-Centre for Microscopy and Spectroscopy with Electrons/ER-C3 Structural Biology, Wilhelm-Johnen-Straße, 52425 Jülich, Germany

⁴Collaboration for joint PhD degree between EMBL and Heidelberg University, Faculty of Biosciences

⁵These authors contributed equally

⁶Lead Contact

*Correspondence: horos@embl.de (R.H.), hentze@embl.de (M.W.H.)

<https://doi.org/10.1016/j.cell.2019.01.030>

SUMMARY

Vault RNAs (vtRNA) are small non-coding RNAs transcribed by RNA polymerase III found in many eukaryotes. Although they have been linked to drug resistance, apoptosis, and viral replication, their molecular functions remain unclear. Here, we show that vault RNAs directly bind the autophagy receptor sequestosome-1/p62 in human and murine cells. Overexpression of human *vtRNA1-1* inhibits, while its antisense LNA-mediated knockdown enhances p62-dependent autophagy. Starvation of cells reduces the steady-state and p62-bound levels of vault RNA1-1 and induces autophagy. Mechanistically, p62 mutants that fail to bind vtRNAs display increased p62 homo-oligomerization and augmented interaction with autophagic effectors. Thus, *vtRNA1-1* directly regulates selective autophagy by binding p62 and interference with oligomerization, a critical step of p62 function. Our data uncover a striking example of the potential of RNA to control protein functions directly, as previously recognized for protein-protein interactions and post-translational modifications.

INTRODUCTION

Vault RNAs (vtRNA) have been described as small non-coding RNA components of giant ribonucleoprotein particles (RNPs), termed vaults (Kedersha and Rome, 1986). Humans express four vtRNA paralogs (*vtRNA1-1*, *vtRNA1-2*, *vtRNA1-3*, *vtRNA2-1*), which are 88–100 nt long and transcribed by RNA polymerase III. Vaults are found in a broad spectrum of eukaryotes ranging from protists to mammals (Stadler et al., 2009). Although vaults can occur at 10,000 to 100,000 particles per cell and have been linked to cellular processes like drug resistance, apoptosis, and nuclear transport (Berger et al., 2009), their function remains unclear. Sedimentation ex-

periments showed that only a fraction of vtRNAs is incorporated into vaults (Kickhoefer et al., 1998), suggesting that vtRNAs may have roles outside of vault RNPs. Overexpression of *vtRNA1-1* was shown to be protective against apoptosis in a cellular model of Epstein-Barr virus infection (Amort et al., 2015) and to favor influenza virus replication via PKR deactivation (Li et al., 2015). Yet, the molecular functions of vault RNAs remain undefined.

Macroautophagy (referred to further as autophagy) is an essential cellular process responsible for the recognition, removal and degradation of intracellular components, organelles and pathogens within membrane vesicles termed autophagosomes (Klionsky et al., 2016). The molecular and functional details of the multiprotein complexes that regulate the formation and growth of autophagosomal double-membranes have been intensively studied (for review, see Yin et al., 2016). After encompassing the cargos, autophagosomes close and fuse with lysosomes and degrade their contents to supply amino acids, lipids, and nucleotides for the anabolic needs of cells.

Autophagy was considered to be a non-selective mechanism until the discovery of autophagic receptors with the ability to bind specific autophagic substrates and bring them to the forming autophagosomal membranes via interaction with Atg8-like proteins, including LC3B and GABARAP (Galluzzi et al., 2017). The protein p62 (also known as sequestosome-1 [SQSTM1]) is such an autophagic receptor with a C-terminal ubiquitin binding domain (UBA) and a LC3-interaction motif (LIR) (Pankiv et al., 2007). p62 co-localizes with LC3-positive autophagosomes and is itself degraded in autophagolysosomes (Pankiv et al., 2007; Sahani et al., 2014; Bjørkøy et al., 2005). Thus, determination of p62 protein levels can serve as a proxy for autophagic flux (Klionsky et al., 2016). p62 mostly serves in selective autophagy for the removal of intracellular pathogens (Zheng et al., 2009) and the degradation of intracellular aggregates marked by ubiquitin (Ub) (Pankiv et al., 2007). Among the autophagy receptors, p62 has the distinct property to oligomerize via its N-terminal PB1 (Phox and Bem1p) domain (Ciuffa et al., 2015). Oligomerization is functionally important, as it increases p62 affinity for LC3-positive membranes (Wurzer



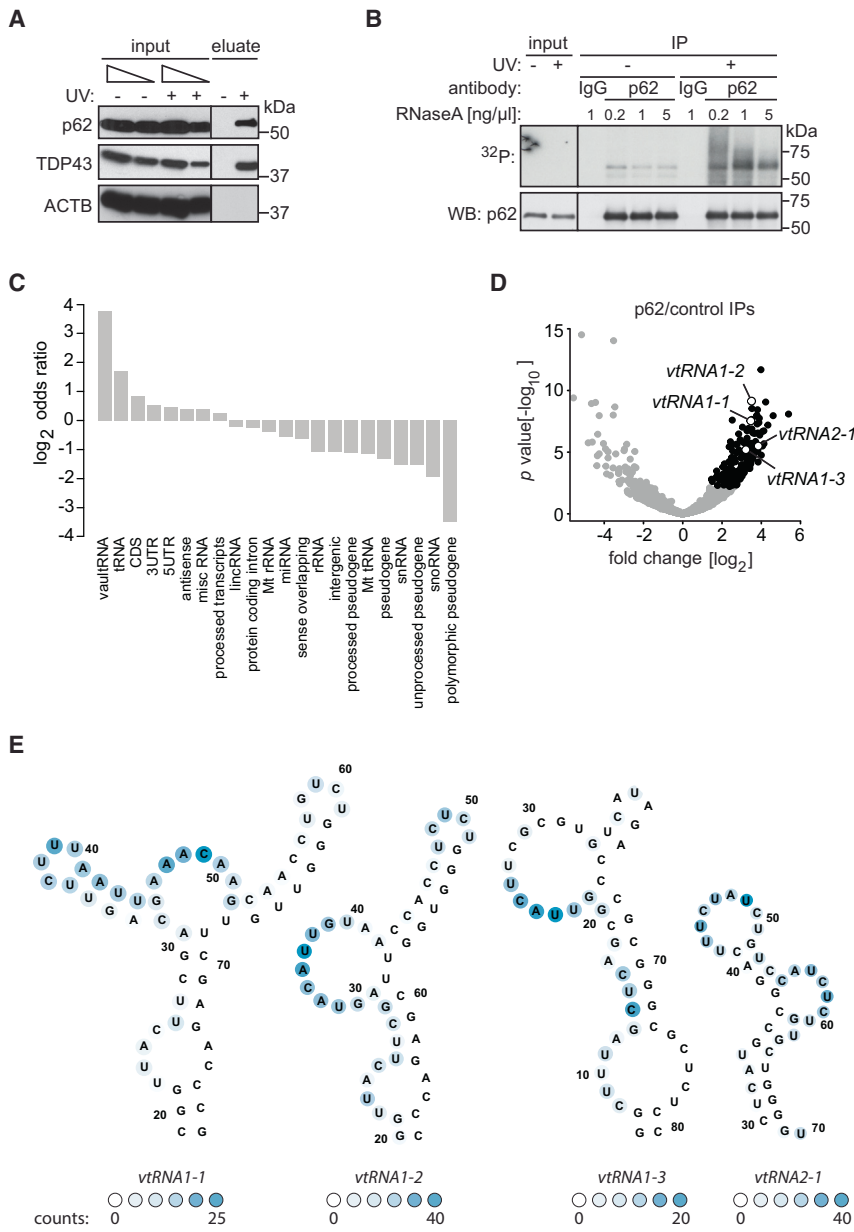


Figure 1. The Autophagy Receptor p62 Is an RNA-Binding Protein

(A) Western blot analysis of input and eluate samples from interactome capture experiment. TDP43 serves as a positive control for RNA binding, whereas actin serves as negative control.

(B) Lysates from UV-treated or control cells were treated with dilutions of RNaseA and used for immunoprecipitation followed by radioactive labeling (upper panel) and western blotting (lower panel).

(C) Log₂ odds ratios of the enrichment of different RNA classes in p62 IPs over the control IPs (Fisher exact test, Benjamini-Hochberg [BH] adjusted p < 0.05).

(D) Volcano plot of differential crosslink site (CS) occurrences; each dot corresponds to a genomic region (exons, introns), black coloring indicates significant enrichment in p62 IPs (BH adjusted p < 0.05). The data were normalized for background and CS enrichment in p62 IPs over controls was tested with DESeq2. Open circles indicate vault RNAs.

(E) Predicted RNA secondary structures of vtRNAs. Mean CS count values in p62 IPs are shown by the indicated color code.

See also Figure S1 and Tables S1, S2, and S3.

Thus, vault RNA1-1 emerges as a riboregulator of targeted autophagy.

RESULTS

The Autophagy Receptor p62/SQSTM1 Is an RNA-Binding Protein

We recently developed a method for the proteome-wide identification of RNA-interacting peptides in RNA-binding proteins (RBPs), termed RBDmap (Castello et al., 2016). We performed RBDmap on human hepatic HuH-7 cells and identified peptides from both known and previously unknown RBPs (<http://www.hentze.embl.de/public/RBDmapHuH7/vignettes/result/>; Table S1). A peptide mapping to the autophagy receptor p62/sequestosome-1 suggested that p62 interacts with RNA. While lysosome-mediated RNA degradation was described long ago (reviewed in Frankel et al., 2017), and autophagy has been implicated in the degradation of ribosomal (Kraft et al., 2008) and retrotransposon RNA (Guo et al., 2014), none of the known mammalian autophagy receptors have been shown to bind RNA directly, which we therefore explored further.

We first validated the p62-RNA interaction. HuH-7 cells were exposed to UV-C light, and covalently bound RNA-binding proteins were recovered from lysates using oligo-(dT) coupled beads (Castello et al., 2013). Western blotting confirmed specific p62 binding to polyadenylated RNA (Figure 1A). In an alternative approach, we UV-C-treated cells followed by lysis

et al., 2015), and is thought to help align p62 to forming autophagosomal structures (Ciuffa et al., 2015). Importantly, oligomerization-deficient p62 is dysfunctional in autophagy (Itakura and Mizushima, 2011). Yet, it is not well understood how the oligomerization of p62 is controlled.

Here, we uncover that the autophagy receptor p62 is an RNA-binding protein. We show that p62 binds the short, non-coding RNA Pol III transcript vault RNA1-1 *in vivo* and *in vitro*. We demonstrate that vault RNA1-1 inhibits p62-dependent autophagy and Ub aggregate clearance, and we show that vault RNA1-1 expression is diminished when autophagy is activated during starvation. Mechanistically, vtRNA1-1 appears to inhibit p62 oligomerization, consequently impairing the binding of p62 to the Atg8-like autophagic effectors LC3B and GABARAP.

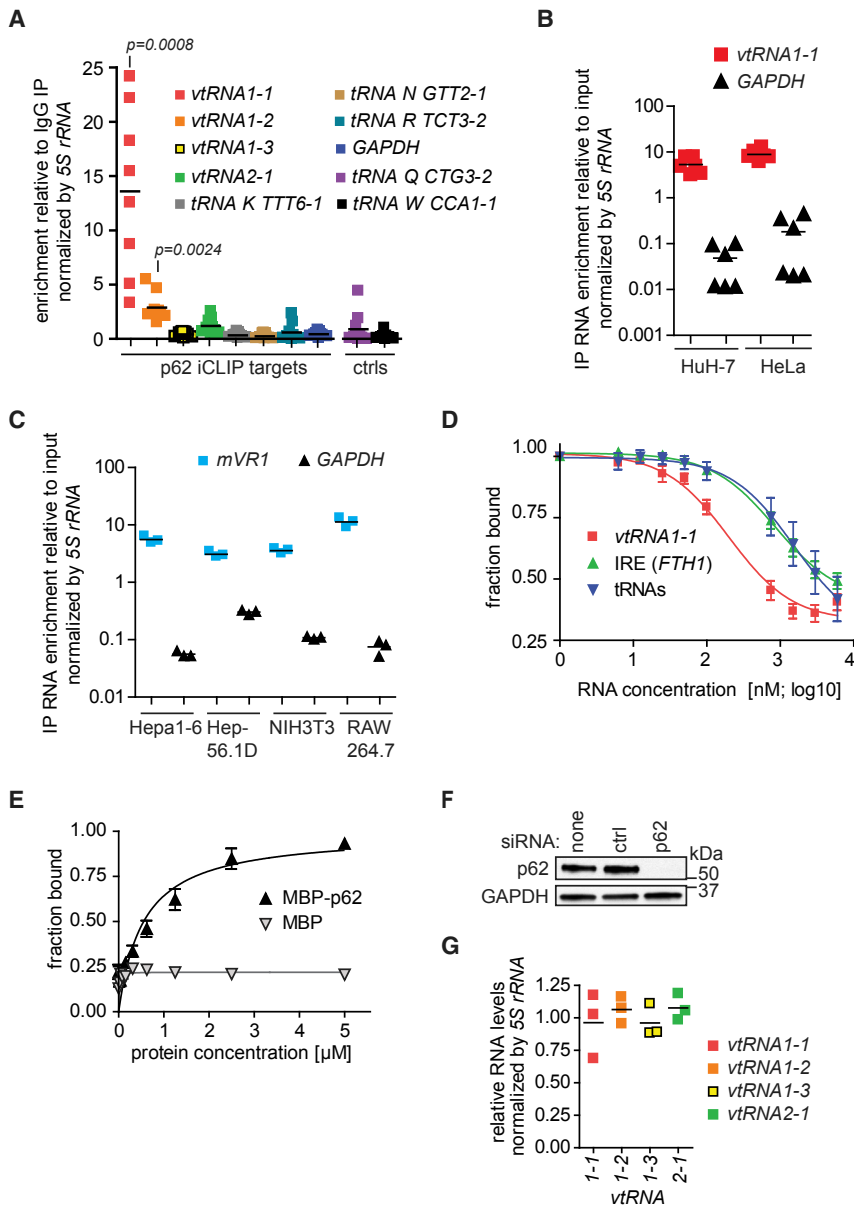


Figure 2. p62 Binds Vault RNA1-1

(A) Differential enrichment of RNAs in native p62 IPs from HuH-7 cells as measured by qRT-PCR. RNA enrichments were normalized by 5S rRNA and compared between p62 and IgG (= 1) IPs. Significant differences are indicated by p values. (B) RNA enrichment in p62 IPs compared to the respective input levels. (C) A representative native p62 IP followed by cDNA synthesis and qRT-PCR measurement. RNA enrichment in p62 IPs compared to the respective input levels. (D) Competition electromobility shift assay (EMSA) using 10 nM of radiolabeled *vtRNA1-1*, 1,500 nM of MBP-p62 protein, and unlabeled competitor RNAs as indicated on the plot; $n = 3$. (E) Determination of RNP complex K_d using EMSA assay with radiolabeled *vtRNA1-1* and MBP-p62 or MBP tag only; $n = 3$. (F) Cells were transfected with indicated siRNAs and lysed after 48 h. Total protein lysates were analyzed by western blotting; a representative image is shown. (G) Total RNA extracted from cells as in (F) was analyzed by northern blotting. Probe signals recognizing respective *vtRNAs* were quantified and normalized by 5S rRNA. Data shown are RNA levels in p62 siRNA-treated cells relative to respective siRNA control.

See also Figure S2 and Table S4.

and RNase treatment. We then immunoprecipitated (IP) p62 and used the IP for radioactive labeling of RNA 5' ends with T4 polynucleotide kinase (PNK) (Baltz et al., 2012). We observed a typical, smeared signal corresponding to RNA-containing complexes, which was reduced to a sharper band depending on the RNase treatment, confirming the p62-cross-linked entity as RNA (Figure 1B). Thus, p62 is a bona fide RNA-binding protein.

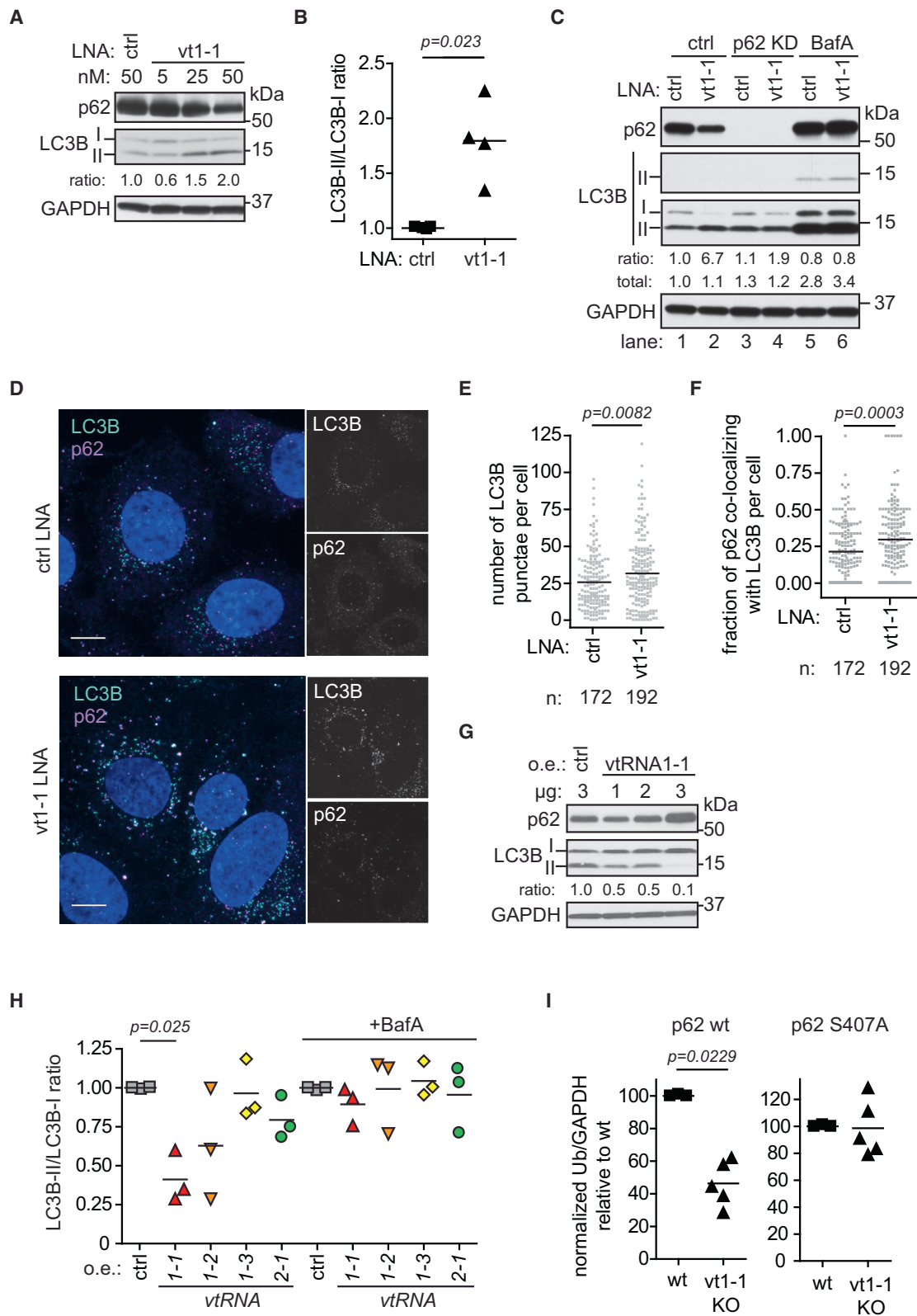
To determine the RNAs bound by p62, we performed iCLIP (Huppertz et al., 2014). We sequenced RNAs that UV-crosslinked to and co-immunopurified with p62 using two independent antibodies (and the respective controls, Figures S1A and S1B), identifying 165 high confidence RNA hits. Among these are numerous polyadenylated transcripts, explaining the initial identification of

p62 as an RBP by RBDmap. However, RNA polymerase III transcripts including tRNAs and vault RNAs emerged as the top categories specifically enriched in the IPs (Figure 1C; Table S2). Differential cross-link site occurrence of individual RNAs isolated from p62 or control IPs, respectively, placed all four human *vtRNAs* prominently on the p62 target list (Figure 1D; Table S3). More detailed analysis of the iCLIP data revealed that p62 preferentially interacts with looped regions of the central domains of the *vtRNAs* (Figures 1E and S1C) without an apparent binding motif.

Thus, p62 predominantly interacts with a subset of Pol III transcripts and shows preferential binding to the central domains of vault RNAs.

Vault RNA1-1 Is a Prime p62-Interacting RNA

To complement the results of iCLIP and to quantify RNA binding to p62 under steady-state conditions, we performed p62 RIP-qPCR (RNP immunoprecipitation followed by cDNA synthesis and quantitative real-time PCR) from HuH-7 cells, using a p62 antibody or control IgG, respectively. We observed prominent and specific enrichment of *vtRNA1-1* relative to the other vault and control RNAs (Figures 2A and S2A). Thus, vault RNA1-1 appears to be a prime interacting RNA of p62.



(legend on next page)

Next, we tested a series of cell lines for the interaction between p62 and *vtRNA1-1* (for human HeLa cells) or the single murine vault RNA *mVR1* in hepatic Hepa1-6 and Hep-56.1D cells, NIH 3T3 fibroblasts, and monocytic RAW264.7 cells by RIP-qPCR. We confirmed p62 binding to *vtRNA1-1* in HeLa cells (Figure 2B) and to *mVR1* in the different mouse cell lines (Figure 2C). Thus, the binding of p62 to vault RNAs is conserved between human and mouse cells.

We next investigated the interaction of p62 and *vtRNA1-1* *in vitro* using an electrophoretic mobility shift assay (EMSA) with purified recombinant protein and radiolabeled *in vitro*-transcribed RNA. Because native p62 tends to oligomerize spontaneously *in vitro* (Ciuffa et al., 2015), we tagged the N terminus with MBP (maltose binding protein; 40 kDa) to prevent spontaneous oligomerization and to facilitate native gel electrophoresis. We observed that MBP-p62 forms complexes with *vtRNA1-1* (Figure S2B). To test whether the interaction between MBP-p62 and *vtRNA1-1* is specific, we used unlabeled *vtRNA1-1* as specific and the iron-responsive element (IRE) from human *FTH1* mRNA or a mixture of bacterial tRNAs, respectively, as non-specific competitors. Unlabeled *vtRNA1-1* effectively competes with the labeled *vtRNA1-1* from p62 ($K_i = 200.7$ nM) as compared to IRE ($K_i = 856.6$ nM) or bacterial tRNAs ($K_i = 1531$ nM) (Figure 2D). We next determined the apparent K_d of p62-*vtRNA1-1* complex formation in the presence of non-specific competitor and determined it to be 546.3 ± 106.6 nM, while the MBP tag alone did not yield any shifted complexes (Figures 2E and S2C). These findings confirm that p62 specifically binds *vtRNA1-1* *in vitro*, complementing our *in cellulo* data (Figures 1 and 2A–2C).

***vtRNA1-1* Inhibits p62-Mediated Autophagy and Ub Aggregate Clearance**

To uncover the functional significance of the *vtRNA1-1*/p62 interaction, we first tested whether p62 might mediate the lysosomal degradation of vault RNAs. However, no difference in the steady-state levels of the vtRNAs could be seen in cells depleted of p62 by small interfering RNA (siRNA) treatment (Figures 2F and 2G) or in p62 KO cells (Figure S2D), respectively. Thus, neither acute nor sustained p62 deficiency affects the steady-state levels of the vault RNAs.

Because p62 binding does not overtly affect the expression of its major class of RNA binders, we next explored whether *vtRNA1-1* conversely might affect p62 function in autophagy. We knocked down *vtRNA1-1* with antisense LNAs, and monitored autophagic flux by assessing two parameters, LC3B conjugation from LC3B-I to LC3B-II during autophagosome assembly, and p62 levels reflecting its autolysosomal degradation. Interestingly, *vtRNA1-1* knockdown (KD) (Figures S3A and S3B) stimulated LC3B conjugation (compare the ratios of LC3BII over LC3BI, Figures 3A and 3B), suggesting increased autophagic flux. In keeping with this notion, we observed a dose-dependent decrease in p62 levels (Figure 3A). To examine whether this effect is dependent on p62, we concurrently removed p62 and *vtRNA1-1*. We observed that removal of p62 partially restores the LC3B conjugation ratio after *vtRNA1-1* depletion compared to controls (Figure 3C, compare lanes 3 and 4 with 1 and 2). Treatment with baflomycin A₁ (BafA), an inhibitor of autophagosome-lysosome fusion and lysosomal degradation that leads to the accumulation of autophagosomes (Klionsky et al., 2016), restored the LC3B conjugation ratio and led to the expected accumulation of total LC3B in *vtRNA1-1* KD cells (Figure 3C, lanes 5 and 6). In addition, immunofluorescence microscopy of cells depleted for *vtRNA1-1* revealed an increased number of LC3B puncta compared to controls (Figures 3D and 3E), and the fraction of p62 co-localizing with LC3B increased upon *vtRNA1-1* KD (Figures 3D and 3F), providing independent evidence for the stimulation of autophagic flux upon *vtRNA1-1* KD. We also corroborated these results by assessing the expression levels of another Atg8-like protein, GABARAP (Figure S3C).

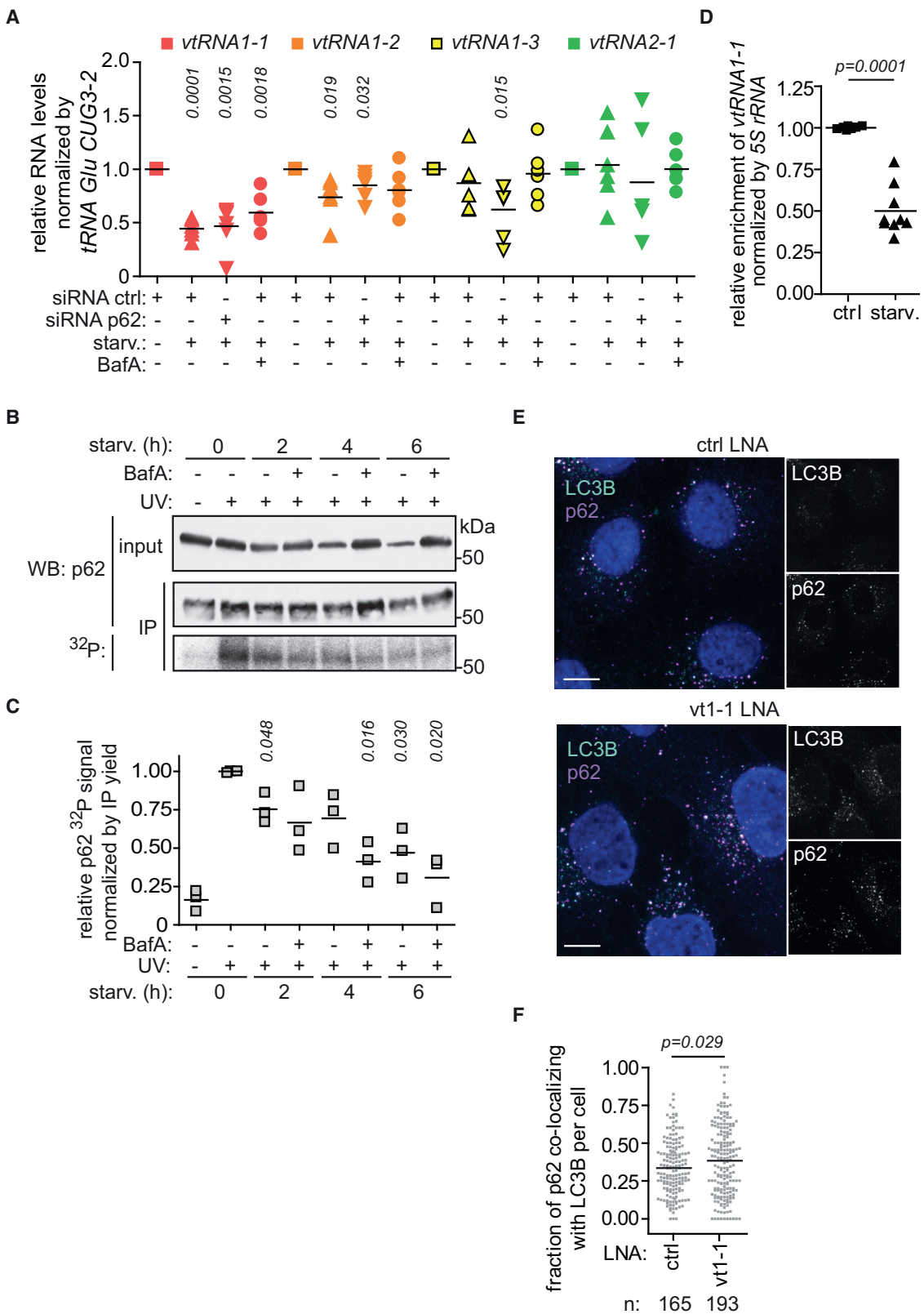
The phosphorylation of the mTORC1 targets ULK1 or 4E-BP1 was not noticeably affected by *vtRNA1-1* KD, suggesting that the effect on autophagy is not the result of decreased mTORC1 activity (Figure S3C). Thus, multiple lines of evidence show that sequestration of *vtRNA1-1* induces autophagic flux in a p62-dependent way.

We also tested whether the increased expression of *vtRNA1-1* by transfection affects autophagy. Elevation of *vtRNA1-1* levels suppresses LC3B conjugation and yields a concomitant accumulation of p62 in a dose-dependent manner (Figures 3G and S3D), both suggesting decreased autophagic flux.

Figure 3. *vtRNA1-1* Regulates p62-Dependent Autophagy and Aggregates Clearance

- (A) HuH-7 cells were transfected with a control LNA oligo or with increasing amounts of an LNA oligo targeting *vtRNA1-1* and lysed after 48 h. Lysates were analyzed by western blotting with the indicated antibodies.
- (B) Quantification of LC3 conjugation from independent experiments using 50 nM LNA transfections.
- (C) Cells were transfected with the indicated LNAs and control or p62 siRNA, and incubated for 48 h. Where indicated, cells were treated with BafA. Lysates were analyzed by western blotting with the indicated antibodies.
- (D) Representative IF images of cells treated as in (B). Cyan, LC3B; magenta, p62; blue, DNA; white, p62/LC3B co-localization. Scale bar, 20 μ M.
- (E) LC3B punctae quantitative image analysis of 2 independent experiments as in (D), n indicates the number of cells analyzed.
- (F) p62 and LC3B co-localization quantitative image analysis of data as in (E).
- (G) HuH-7 cells were transfected with empty vector (ctrl) or plasmid encoding *vtRNA1-1* and lysed after 24 h. Lysates were analyzed by western blot with the indicated antibodies.
- (H) Cells were transfected with indicated *vtRNA*-encoding plasmids, vehicle-treated or treated with BafA at 100 nM for 5 h, and then lysed. Lysates were analyzed by western blotting and images of LC3B staining were quantified.
- (I) HuH-7 WT or *vtRNA1-1*KO cells were treated with siRNA against p62, and p62 WT or p62 S407A, respectively, was expressed by transfection of siRNA-resistant cDNA expression vectors. Cells were then vehicle-treated or treated with 0.25 μ M of MG132 overnight, lysed, and analyzed by western blotting. Quantification of western blots for anti-ubiquitin normalized by GAPDH expression is plotted as fold changes compared to HuH-7 WT vehicle control sample; n = 3.

See also Figure S3.



(legend on next page)

Overexpression of other vault RNAs did not consistently affect the LC3B conjugation ratio (Figures 3H and S3D). BafA treatment restored the LC3B conjugation ratio in cells overexpressing *vtRNA1-1* (Figure 3H), suggesting that *vtRNA1-1* overexpression does not disturb LC3 conjugation per se, but rather restricts autophagic flux.

Last, we investigated whether p62-dependent Ub aggregate clearance is affected by *vtRNA1-1*. We treated HuH-7 wild-type (WT) and *vtRNA1-1*KO cells (Figures S6B–S6D), respectively, with the proteasome inhibitor MG132 and assessed Ub-positive aggregate levels by western blotting. In cells lacking *vtRNA1-1*, aggregate accumulation is significantly reduced when p62 WT protein is present (Figure 3I). However, the p62 S407A variant that does not undergo ULK1-dependent phosphorylation and activation of the UBA domain (Lim et al., 2015) fails to mediate better aggregate clearance in *vtRNA1-1*KO cells (Figure 3I), showing that the observed difference between WT and *vtRNA1-1*KO cells in aggregate clearance is mediated by p62.

Taken together, experimental up- or down-modulation of *vtRNA1-1* levels inversely affect p62-dependent autophagy and p62-dependent aggregate clearance.

***vtRNA1-1* Levels and p62 RNA Binding Are Dynamically Regulated by Starvation**

Next, we explored whether the regulatory potential of the p62 and *vtRNA1-1* interaction is used physiologically. Amino acid and serum starvation induce autophagy, where p62 supports the increased autophagic flux (Bjørkøy et al., 2005) and undergoes degradation itself (Sahani et al., 2014). HuH-7 cells cultivated in minimal media lacking amino acid and serum respond with a major drop in *vtRNA1-1* levels after 6 h of starvation (Figures 4A and S4A). This decrease in *vtRNA1-1* levels is not a result of autophagic co-degradation with p62, because neither the KD of p62 nor BafA treatment significantly restored *vtRNA1-1* levels (Figure 4A). Interestingly, the specific, starvation-induced decrease in *vtRNA1-1* levels is also observed when the RNA is expressed from a heterologous (H1) promoter (Figure S4B), suggesting that the regulatory information is contained within the gene body of *vtRNA1-1*. Whether regulation is exerted transcriptionally via the internal Pol III promoter sequences and/or post-transcriptionally at the RNA level remains to be determined. We also assessed a starvation time course of the levels of several tRNAs, which further attests to the specificity of the response of *vtRNA1-1* (Figure S4C).

RNA binding of p62 follows the diminished *vtRNA1-1* expression in the course of starvation (Figures 4B and 4C). Cells starved in the presence of BafA, which prevents p62 degradation, show that bulk autophagy decreases the fraction of RNA-bound p62 relative to total p62. BafA treatment per se in complete medium does not change the RNA binding properties of p62 (Figure S4D), suggesting that the effect on RNA binding is not driven by p62 protein levels. Therefore, p62 active in autophagy and destined for lysosomal degradation apparently does not bind RNA, in keeping with the notion that RNA binding inhibits p62 function in autophagy.

Of note, the starvation-induced decrease in *vtRNA1-1* levels correlates with a decrease in the fraction of RNA-bound p62 (Figure S4E). Importantly, starvation reduces the interaction of p62 and *vtRNA1-1* (Figure 4D), and removal of *vtRNA1-1* by LNA KD prior to starvation further potentiates interaction of p62 with LC3B (Figures 4E and 4F). It thus appears that at least part of the starvation-mediated activation of autophagy includes the removal of inhibitory *vtRNA1-1* from p62.

Collectively, these data show that *vtRNA1-1* levels and the interaction of *vtRNA1-1* with p62 are physiologically regulated by amino acid and serum starvation.

p62 Binds *vtRNA1-1* Primarily via Its Zinc Finger Domain

To study the mechanism of how *vtRNA1-1* inhibits p62 function, we wanted to generate an RNA binding-deficient mutant of p62. p62 possesses several domains with assigned functions and interaction partners, but no classical RNA-binding motif (Figure 5A). To identify the RNA-binding region of p62, we utilized our RBDmap data and inspected the neighboring region of the RBDpep (Castello et al., 2017) that we had identified within the ZZ domain (Figure 5A and 5B). We found that substitution of the conserved K141 within the ZZ domain of p62 by alanine appeared to decrease RNA binding (Figure S5A), but complex formation between the endogenous WT p62 with the stably expressed p62 K141A variant interfered with the analysis. We therefore depleted endogenous p62 from HuH-7 cells by RNAi and transfected tagged p62 variants resistant to the siRNAs by synonymous mutations. As expected, siRNA KD of p62 effectively removed its radiolabeling signal (Figure 5C, lanes 1, 2). The p62 K141A variant displays strongly reduced RNA binding compared to the WT, which is further diminished in the R139/K141/AA variant (referred to as p62 RK/A, Figure 5C, lanes 3–5). The shift of tagged p62 by 2.5 kDa, both on the PNK assay and the western blot, also provides evidence that RNA binding of p62 is direct.

Figure 4. Starvation Reduces p62 RNA Binding and *vtRNA1-1* Expression

(A) HuH-7 cells were treated with a control siRNA or p62 siRNA for 48 h, followed by starvation for 6 h. Total RNA was isolated and analyzed by northern blotting; phosphorimages were quantified, and data were plotted as relative to non-starved samples. Significant differences to respective non-starved samples are indicated by p values; n = 6.

(B) Cells were starved in medium containing solvent control or BafA at 100 nM for the indicated time, 254 nm UV-C light exposed, and lysed. Lysates were used for p62 IP and RNA radiolabeling assay. After SDS-PAGE and transfer, the membrane was exposed overnight on film and used subsequently for western blotting.

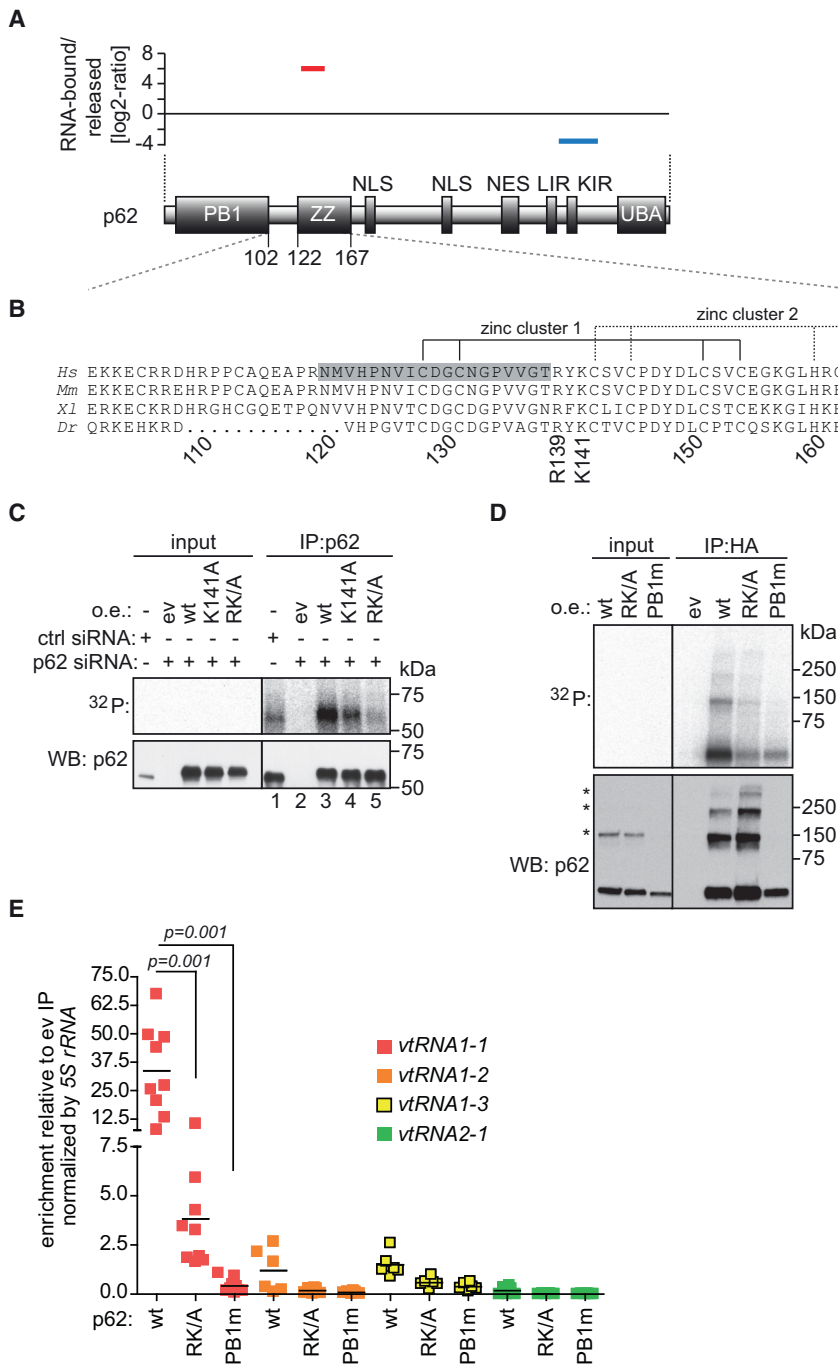
(C) Phosphorimages and western blots of 3 independent replicates as described in (B) were used for quantification. Significant differences to the 0 h sample are indicated by p values.

(D) Enrichment of *vtRNA1-1* on native p62 IPs from cells cultured in complete media or starvation media for 2 h.

(E) Cells were transfected with the indicated LNAs, incubated for 48 h, and then starved for 2 h. Representative IF images of cells are shown. Cyan, LC3B; magenta, p62; blue, DNA; white, p62/LC3B co-localization. Scale bar, 20 μ M.

(F) Image analysis and quantification of cells as in (E) using 2 independent experiments; n indicates the number of cells analyzed.

See also Figure S4.



Next, we generated HuH-7 p62 KO clones using CRISPR/Cas9 gene inactivation (Figures S5B and S5C) and confirmed the decreased RNA binding of p62 RK/A in a p62 null background (Figure S5D). To investigate whether oligomerization of p62 may affect RNA binding, we expressed an oligomerization-deficient variant of p62 (Lamark et al., 2003), a triple mutation R21A, D69A, D73A, referred to as p62 PB1m. p62 PB1m also showed diminished RNA binding (Figure 5D). Even if RNA binding of p62 PB1m is less compromised

Figure 5. p62 Binds vtRNA1-1 Primarily via Its Zinc Finger Domain

(A) RBDmap-enriched peptide (red) and a peptide not enriched in the RNA-bound fraction (blue) positioned on the p62 protein. The x axis is scaled to protein length. A scheme of the p62 domain architecture is drawn below. NLS, nuclear localization signal; NES, nuclear export signal, LIR, LC3 interaction region; KIR, Keap1 interaction region; UBA, ubiquitin associated domain.

(B) Human p62 protein region between AA 101–163. Orthologous proteins are aligned below; the dotted region represents the insertion of a longer peptide. The RBDmap-enriched peptide (FDR 1%) is shaded in gray. *Hs*, *Homo sapiens*, *Mm*, *Mus musculus*, *Xl*, *Xenopus laevis*, *Dr*, *Danio rerio*.

(C) HuH-7 cells treated with the indicated siRNA were transfected with empty vector (ev) or p62 WT and variants (K141A, RK/A refers to the R139/K141-AA) cDNAs resistant to RNAi. Cells were exposed to 254 nm UV-C light, lysed, and used for IP followed by the radioactive labeling of RNAs and western blotting.

(D) HuH-7 p62KO cells were transfected with empty vector (ev) or p62 WT and variants (RK/A; PB1m refers to triple mutation in PB1 domain). Cells were exposed to 254 nm UV-C light, lysed, and used for IP followed by the radioactive labeling of RNAs and western blotting.

(E) Differential enrichment of indicated RNAs on HA IPs from p62 KO cells expressing transfected p62 variants. RNA enrichment levels measured by qRT-PCR normalized to 5S rRNA were compared to ev enrichment (= 1). Significant differences between the p62 variants are indicated by p values.

See also Figure S5.

than that of the p62 RK/A variant (Figure S5D), its diminished RNA interaction compared to the WT protein suggests that the PB1 domain contributes to RNA binding.

To quantify the RNA binding of the p62 variants to vault RNA, we expressed HA-tagged p62 variants in HuH-7 p62 KO cells (Figure S5E), and used the lysates for IP followed by qPCR. As is the case for endogenous p62 protein, tagged WT p62 strongly interacts with vtRNA1-1, while the p62 RK/A mutant and the PB1m variant display strongly reduced vtRNA1-1 binding (Figure 5E), suggesting that both domains contribute to full vault RNA1-1 binding.

vtRNA1-1 Regulates the Interaction of p62 with Atg8-like Proteins

With the RK/A mutant available, we could address the mechanism of vtRNA1-1 function. We first tested whether RNA binding affects interactions of p62 with the Atg8-like proteins LC3B and GABARAP by co-immunoprecipitation (coIP). Both proteins

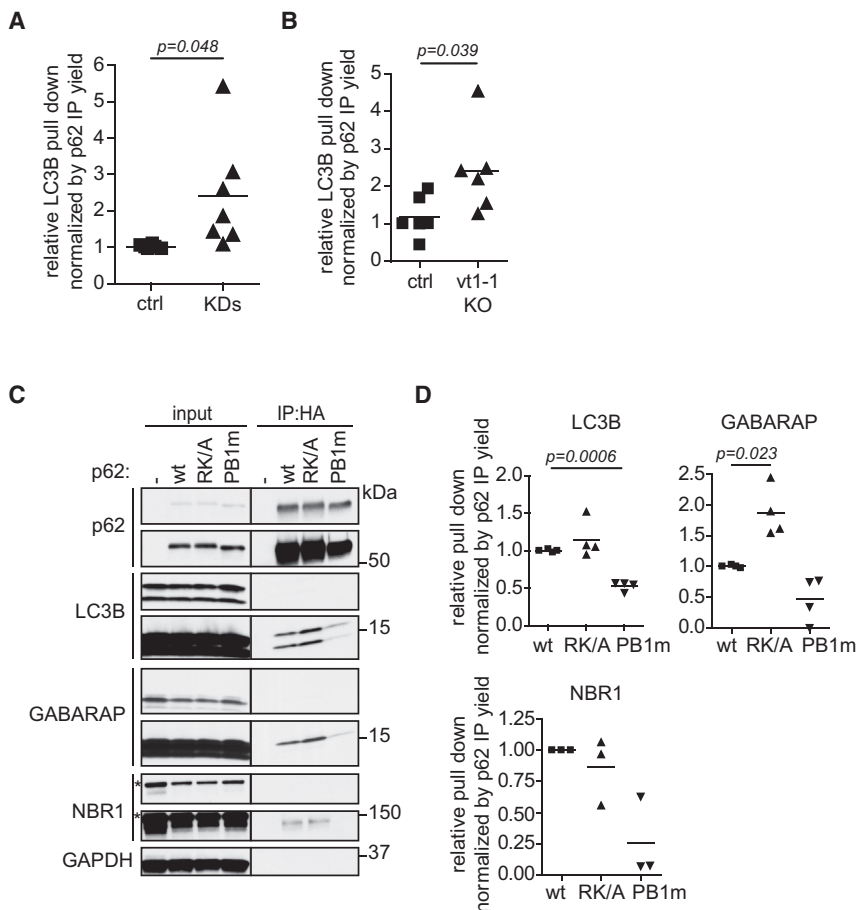


Figure 6. vtRNA1-1 Affects p62 Interactions with Atg8-like Proteins

(A) HuH-7 cells were transfected with the ctrl LNA or LNA targeting *vtRNA1-1*, cultured for 48 h, and then treated with 100 nM BafA for 5 h. Cells were subjected to DSP protein-protein crosslinking, lysed, and used for p62 IPs. Eluates from IPs were analyzed by western blotting and quantified.

(B) p62 coIP analysis of controls and *vtRNA1-1* KO cells, performed as in (A).

(C) HuH-7 p62KO cells were transfected with the indicated p62 variants, cultured for 24 h, and then treated with 100 nM BafA for 5 h. Cells were subjected to DSP protein-protein crosslinking, lysed and used for IPs. Eluates from IP were analyzed by western blotting. *Indicates a non-specific band.

(D) Quantification of pull-down efficiency of replicate experiments as shown in (C). See also Figure S6.

interaction with the autophagic machinery (Itakura and Mizushima, 2011).

Because removal of vault RNA1-1 or rendering p62 RNA binding-deficient both increase p62's engagement with LC3B and GABARAP, the data suggest that vault RNA1-1 binding affects the interactions of p62 with Atg8-like proteins.

p62 RNA Binding Inversely Correlates with Its Oligomerization State *In Cellulo*

We then wanted to determine whether the above regulation was a direct or an indirect

effect of vtRNA binding to p62. Further analysis of the data shown in Figure 5D revealed that UV-C exposure of cells to crosslink RNAs to p62 also induces a laddering of the protein on a western blot that persists through denaturing SDS-PAGE (bottom panel). While p62 oligomerization has been studied extensively *in vitro* (Wurzer et al., 2015; Ciuffa et al., 2015; Zaffagnini et al., 2018), little is known about the precise oligomeric state in the cellular context (Carroll et al., 2018). Because the oligomerization-deficient PB1m variant completely lacks this laddering (Figure 5D), serendipitously, we appear to have found direct biochemical evidence for p62 oligomerization in cells and a simple assay for this process. Although UV treatment typically does not induce protein-protein crosslinks (Pashev et al., 1991; Suchanek et al., 2005), the local topology of p62 oligomers may favor reactive oxygen species-induced covalent bond formation between the p62 subunits (Donohue et al., 2014).

To evaluate this laddering assay in a physiological context, HuH-7 cells were starved for 2 h before UV crosslinking, and cell lysates were assessed by the laddering assay and for RNA binding by PNK assay. As expected, starvation reduces p62 RNA binding (Figure 7A, top) and, importantly, increases the laddering of p62 visualized by western blotting (Figure 7A, bottom, compare lane 5 with lane 8). The RK/A variant strikingly displays this enhanced laddering even under basal culture conditions

co-purify with p62 and display the expected increase in interaction when autophagy is induced by starvation (Figure S6A, compare the lanes 2 and 4). Following KD of *vtRNA1-1*, p62 displays increased interaction with LC3B (Figure 6A), corroborating data obtained by immunofluorescence (IF) microscopy. We also prepared HuH-7 *vtRNA1-1* KO cell lines by CRISPR/Cas9 gene deletion. We deleted the *vtRNA1-1* transcription unit (Figure S6B) and verified the specificity of the deletion by genomic PCR (Figure S6C). We confirmed the deletion of *vtRNA1-1* using qRT-PCR on total RNA prepared from the *vtRNA1-1* KO clones (Figure S6D). We also observed increased interaction between p62 and LC3B in cells deleted for the *vtRNA1-1* locus (Figures 6B and S6E). These data suggest that *vtRNA1-1* regulates the interaction of p62 with LC3B.

To test this further, we conducted coIP in HuH-7 p62 KO cells reconstituted with the p62 WT, RK/A, or PB1m variants, respectively. Although the interaction with LC3B is not significantly changed, the p62 RK/A variant shows increased complex formation with the Atg8-like protein GABARAP compared to WT p62 (Figures 6C and 6D). As a control, the interaction with the PB1 domain-binding protein NBR1 is unchanged between the p62 WT and RK/A variant (Figures 6C and 6D). As expected, the p62 PB1m variant displays decreased binding to LC3, GABARAP, and NBR1 (Figures 6C and 6D), reflecting the requirement for p62 oligomerization for efficient

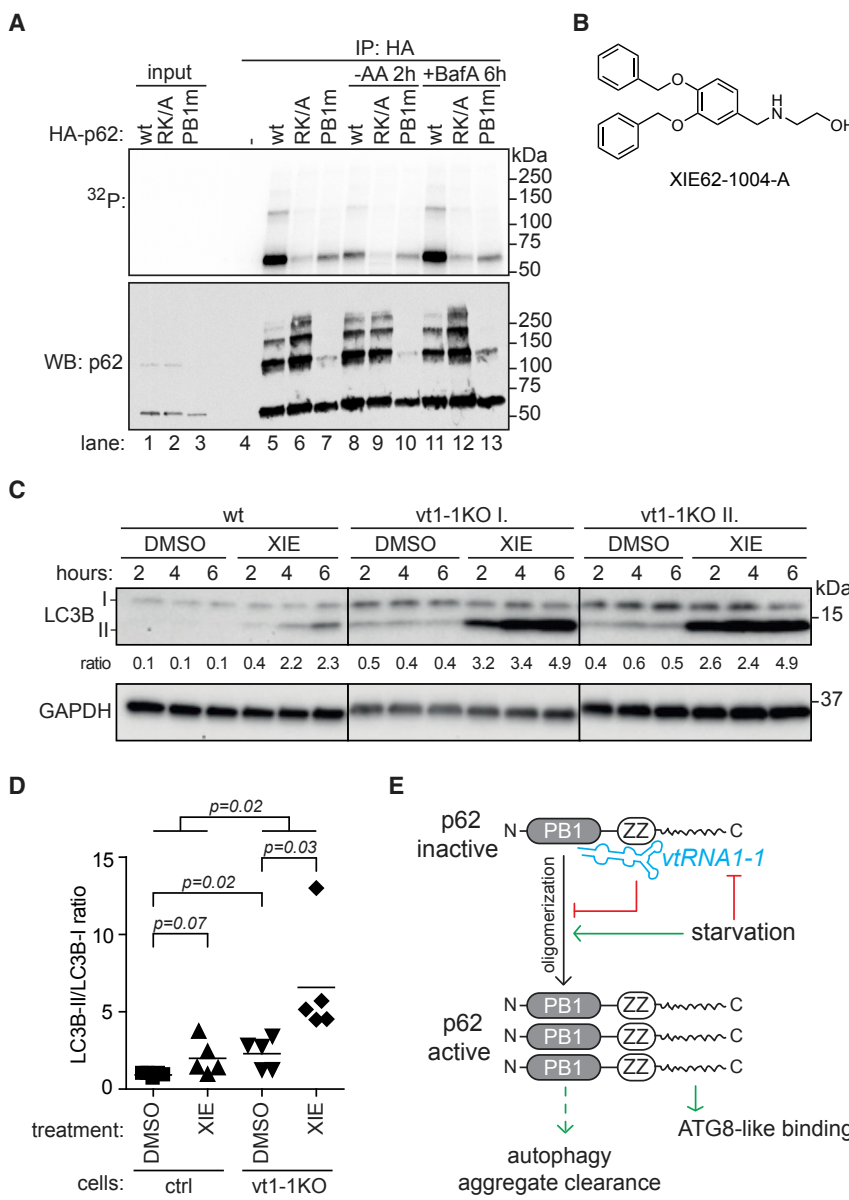


Figure 7. Mechanism of *vtRNA1-1* Function as a Riboregulator of Autophagy

(A) HuH-7 p62KO cells were transfected with the indicated p62 variants, cultured for 24 h, and then cultured in starvation media for 2 h or treated with 100 nM BafA in complete media for 5 h. Cells were exposed to 254 nm UV-C light, lysed, and used for IP followed by the radioactive labeling of RNAs and western blotting.

(B) Chemical structure of XIE62-1004-A (XIE).

(C) HuH-7 WT or vtRNA1-1KO cells were treated with 20 μ M XIE, or solvent, for the indicated times. Cells were then lysed and analyzed by western blotting.

(D) HuH-7 control cells (WT and CRISPR ctrl clones) or vtRNA1-1KO cells, respectively, were treated with 10 μ M XIE or solvent for 1 h, lysed, and analyzed by western blotting. LC3B conjugation ratios from 3 independent experiments are plotted. Significant differences are indicated by p values. The effect of XIE was analyzed by the robust F test.

(E) Working model for the function of *vtRNA1-1* as a riboregulator of p62 protein multimerization and activity.

sessed by LC3B conjugation. As expected, the *vtRNA1-1KO* cells display increased LC3B conjugation compared to their WT counterparts already under control conditions (Figure 7C). In keeping with its original description (Cha-Molstad et al., 2017), XIE treatment induces LC3B lipidation in control cells, and its effect is significantly enhanced in the *vtRNA1-1KO* cells (Figure 7D). Thus, the cellular response to this p62-specific activator of autophagy is strongly affected by *vtRNA1-1* (Figures 7C and 7D), meeting a prediction for a riboregulator of p62 function.

DISCUSSION

Our experiments show that the small non-coding RNA *vtRNA1-1* contributes to the regulation of autophagic flux by direct interaction with the autophagy receptor protein p62/sequestosome-1. Thus, we can assign a mechanism-based function to the first member of the family of vault RNAs, which was described more than 30 years ago (Kedersha and Rome, 1986). Our data also show that a small non-coding RNA can regulate a biological process by directly affecting the function of a protein, which is typically expected of protein-protein interactions.

Vault RNAs, p62, and the Regulation of Autophagy

Autophagy is a highly regulated process, especially at the level of initiation (Sica et al., 2015). We show that starvation triggers a reduction of the steady-state levels of *vtRNA1-1* (Figures 4A and S4A–S4C) and diminishes *vtRNA1-1* binding to p62 (Figures 4B–4D). Gain- and loss-of-function

(lane 6), which is not increased further by starvation (lane 9). Thus, the RK/A mutant oligomerizes under basal conditions like WT p62 after starvation, strongly suggesting that *vtRNA1-1* interferes with p62 oligomerization. We also note that the p62 oligomers display profoundly reduced RNA binding compared to monomeric p62 (Figures 5D and 7A, compare the top and the bottom panels), which indicates that p62 monomers or low complexity oligomers represent the RNA-binding forms of p62.

Finally, we used XIE62-1004-A (XIE, in short) (Figure 7B), a small molecule that binds to the ZZ-domain of p62, inducing p62 oligomerization and activating p62-dependent autophagy (Cha-Molstad et al., 2017). XIE thus affords an opportunity to directly test p62-dependent autophagy in addition to starvation-induced autophagy, which is more pleiotropic. HuH-7 WT or vtRNA1-1KO cells were treated with XIE, or solvent control, and autophagy was as-

experiments demonstrate that *vtRNA1-1* negatively controls p62 in autophagy (Figure 3). This conclusion is corroborated by analyses of the RNA binding-deficient RK/A mutant of p62, which shows characteristics of activated p62 even under non-starvation conditions (Figures 6D, 6E, and 7A). The starvation-induced drop in *vtRNA1-1* levels thus contributes to the physiological, p62-mediated increase in autophagic flux.

Future work will address how starvation signals control *vtRNA1-1* expression. Conceivably, both transcriptional and/or post-transcriptional mechanisms could contribute to this control. Pol III transcription is controlled by the repressor protein MAF1, which in turn is inhibited by phosphorylation via mTORC1 (Orioli et al., 2016). Whether MAF1-inhibition may be selective for *vtRNA1-1* transcription compared to the other vault RNA genes remains to be investigated. Alternatively, cytosine-5 methylation at position C69 of *vtRNA1-1* was shown to promote processing of *vtRNA1-1* into small vault RNAs (svRNAs) (Hussain et al., 2013), effectively reducing the pool of *vtRNA1-1*. It will be interesting to investigate *vtRNA1-1* processing in the context of starvation. In any case, because *vtRNA1-1* expressed from a heterologous promoter is specifically and strongly regulated by starvation (Figure S4B), the *cis*-regulatory information is embedded within the DNA and/or RNA sequence of *vtRNA1-1* itself.

While our experiments explore starvation, proteasome inhibition, and pharmacological induction by XIE62-1004-A as triggers of p62-dependent autophagy, we have not tested other conditions that affect autophagy so far. It will be informative to investigate whether, e.g., p62-dependent xenophagy (Galluzzi et al., 2017), is affected by *vtRNA1-1*. It will also be relevant to investigate possible functions of the other RNAs that bind p62, including the three additional human vault RNAs. Upregulation of a *vtRNA2-1* fragment (svtRNA2-1a) was found to mark early stages of Parkinson disease (PD) and to induce neuronal dysfunction (Miñones-Moyano et al., 2013). Intracellular protein inclusions that are typical of PD commonly contain p62 (Zatlowka et al., 2002), and it is possible that RNA binding by p62 could play a role in PD.

Vault RNAs and vault particles are highly expressed in cells and processes that are strongly linked to autophagy. These include *Dictyostelium discoideum* (Vasu et al., 1993) and macrophages (Izquierdo et al., 1996), highly autophagic or phagocytic cells, and several multi-drug-resistant cancer cells (Berger et al., 2009). Epstein-Barr virus (EBV) potently induces *vtRNA1-1* expression, which potentiates viral replication and protects infected cells from apoptosis (Amort et al., 2015; Nandy et al., 2009). Induced expression of *vtRNA1-1* also increases viral titers of influenza A in cell culture models and *in vivo* (Li et al., 2015). Interestingly, both EBV and influenza A infections can block autophagosome maturation and turnover, respectively (Jackson, 2015). Whether p62 is involved in these responses remains to be investigated. Because p62 is involved in other cellular processes including oxidative stress response (Komatsu et al., 2010), mTORC1 regulation (Duran et al., 2011), or nuclear factor κ B (NF- κ B) signaling (Durán et al., 2004), it will also be meaningful to explore the role of RNA binding in these settings.

A Mechanistic Model for p62 Regulation by *vtRNA1-1*

Mutagenesis experiments based on RBDmap data identified a critical role of the ZZ domain of p62 in RNA binding (Figure 5). Interestingly, a PB1 domain mutant of p62 bearing an intact ZZ domain also displays compromised RNA-binding activity (Figures 5D and 5E), suggesting that the PB1 domain may also interact with RNA or that oligomerization is required for RNA binding. In favor of the former explanation, PNK assays show strong RNA binding for monomeric and low complexity oligomeric p62, but hardly any for higher complexity multimers (Figures 5D and 7). The results of EMSA assays support this interpretation (Figures S2B and S2C). We suggest that *vtRNA1-1* binds to monomeric, dimeric, or low complexity oligomeric p62 and interferes with subsequent p62 multimerization. This interference is evident from the increased oligomerization of p62 when *vtRNA1-1* expression is diminished during starvation (Figure 7A), when *vtRNA1-1* binding is impaired due to the RK/A mutation (Figure 7A), and when the oligomerization-inducing ligand XIE is used (Figures 7C and 7D). Therefore, we propose that *vtRNA1-1* interferes with p62 multimerization, which is in turn required for the localization of p62 to autophagosomes and its interaction with the Atg8-like proteins LC3B and GABARAP (Itakura and Mizushima, 2011).

We have no evidence to believe that *vtRNA1-1* acts as a dominant “on-off switch” of p62 activity. We rather envisage *vtRNA1-1* to function as a “p62 activity dial” that is itself regulated by biological cues such as starvation and that modulates the activity of p62 as an autophagy receptor by controlling its multimerization. While our data implicate p62 as the direct and primary target of *vtRNA1-1* in autophagy, we cannot exclude additional regulatory roles of *vtRNA1-1* in this process. In fact, knockdown of p62 by RNAi did not fully restore the LC3B lipidation ratio following *vtRNA1-1* knockdown (Figure 3C), reflecting the incomplete removal of p62 by RNAi and/or implicating additional autophagic targets of *vtRNA1-1*.

We currently do not know the precise features of *vtRNA1-1* that determine its specific binding to p62. Our iCLIP data indicate that p62 primarily binds to the central regions of the different human vault RNAs (Figures 1E and S1C). We also found that the single murine *mVR1* vault RNA binds p62 in several cell lines that we tested (Figure 2C). We have not yet recognized a shared feature of *vtRNA1-1* and *mVR1* RNAs that distinguishes these from the other three human vault RNAs. While iCLIP showed that p62 interacts with all four human vault RNA paralogs (Figures 1D and 1E), the RIP-qPCR data show that *vtRNA1-1* is the predominant p62 target (Figures 2A and 5E). We hypothesize that a cellular factor may contribute to the selectivity of p62 for *vtRNA1-1* under steady-state conditions. Mutagenesis experiments and high resolution structural analyses are expected to shed light on the exact mode of interaction between p62 and *vtRNA1-1*, with implications for both the question of determinants of binding specificity and the mechanistic model discussed above.

It will also be important to determine whether *vtRNA1-1* binds to and inhibits p62 as a “free” RNA or as part of the vault particle. A large fraction of vault RNAs is not associated with the vault particle in different cell types (Kickhoefer et al., 1998), and both possibilities therefore need to be considered. At least *in vitro*, non-particle associated *vtRNA1-1* can bind to p62. Moreover, p62 co-immunoprecipitation experiments that yield *vtRNA1-1* and the Atg8-like

proteins (Figure 6) have failed to identify the major vault protein (data not shown) as an interactor. While this indirect evidence points to the free, non-particle associated RNA as the regulator of p62, the question remains to be answered formally.

Beyond p62 and Vault RNA

Recent work from several laboratories identified hundreds of proteins that had previously escaped detection as RNA-binding proteins (reviewed in Hentze et al., 2018). Many of these RBPs lack classical RNA-binding domains and assigned functions in RNA biology; we collectively refer to these as enigmRBPs (Beckmann et al., 2015). The intensively studied p62/sequestosome-1 is an excellent example of such an enigmRBP, whose RNA-binding properties was previously undiscovered.

The regulation of protein function by an RNA, as seen for p62/vtRNA1-1, could represent a general principle of biological control, complementing well-recognized forms of regulation such as by protein-protein interactions and post-translational modifications. In bacteria, 6S RNAs are 180–200 nt-long RNAs that bind and regulate RNA polymerase activity during the stationary growth phase (Wassarman and Storz, 2000). In mammalian cells, innate immune effector proteins such as Toll-like receptors or the protein kinase PKR sense the presence of viral RNAs, leading to their activation (Kato et al., 2011; Meurs et al., 1990). vtRNA1-1 acts as a physiological “riboregulator” that controls a cellular process, such as autophagy, by direct binding to the autophagy receptor p62. We predict that the regulatory principle employed by p62/vtRNA1-1 will be found to be more widespread in biology, especially among enigmRBPs.

STAR★METHODS

Detailed methods are provided in the online version of this paper and include the following:

- **KEY RESOURCES TABLE**
- **CONTACT FOR REAGENT AND RESOURCE SHARING**
- **EXPERIMENTAL MODELS AND SUBJECT DETAILS**
- **METHOD DETAILS**
 - Transfections and treatments
 - RNA interactome capture
 - Polynucleotide kinase (PNK) assay
 - p62 iCLIP
 - Native p62 IP and protein-protein co-IP
 - qRT-PCR
 - RNA isolation and Northern blotting
 - RBDmap
 - Protein extracts, SDS-PAGE and western blotting
 - siRNA, LNAs
 - Cloning
 - CRISPR/Cas9 gene deletion of vtRNA1-1
 - CRISPR/Cas9 mediated p62 gene inactivation
 - *In vitro* transcription and EMSA
 - p62 protein expression and purification
 - Immunofluorescence microscopy and image analysis
 - Chemical synthesis of XIE62-1004-A
- **QUANTIFICATION AND STATISTICAL ANALYSIS**
- **DATA AND SOFTWARE AVAILABILITY**

SUPPLEMENTAL INFORMATION

Supplemental Information includes six figures and four tables and can be found with this article online at <https://doi.org/10.1016/j.cell.2019.01.030>.

ACKNOWLEDGMENTS

We are grateful to Bernd Fischer for the analysis of the RBDmap dataset, to Bernd Klaus (Centre for Statistical Data Analysis, EMBL) for help with statistical analyses, to Charles Girardot (Genome Biology Computational Support, EMBL) for help with sequencing data deposition, to Malte Paulsen (Flow Cytometry Core Facility, EMBL) for FACS sorting, to the Advanced Light Microscopy Facility (ALMF, EMBL) for microscopy support, to the Centre for Bioimage Analysis (CBA, EMBL) for image analysis support, to Mairi Clarke for protein purification assistance, and to members of the Hentze group for critical reading of the manuscript. This work was supported by a European Research Council Advanced Grant and by a grant from the Virtual Liver Consortium (German Ministry for Education and Research) (to M.W.H.). D.D. was supported by a fellowship from the EMBL Interdisciplinary Postdoc (El3POD) programme under Marie Skłodowska-Curie Actions COFUND (664726).

AUTHORS CONTRIBUTIONS

R.H. and M.W.H. designed the project. R.H., M.B., R.K., and A.-M.A. performed most of the experiments. A.K.T. performed protein *in vitro* purifications. T.S. analyzed the sequencing data. D.D. synthesized XIE62-1004-A. C.T. analyzed the imaging data. E.M.Z. set up immunofluorescence microscopy. A.A. performed interactome capture. A.C. performed RBDmap. R.H., M.B., W.H., C.S., and M.W.H. performed the data analysis. R.H. and M.W.H. wrote the manuscript with input from all authors.

DECLARATION OF INTERESTS

The authors declare no competing financial interests. Aspects of this work have been included in patent application EP3263704A1.

Received: May 14, 2018
 Revised: October 15, 2018
 Accepted: January 16, 2019
 Published: February 14, 2019

REFERENCES

- Amort, M., Nachbauer, B., Tuzlak, S., Kieser, A., Schepers, A., Villunger, A., and Polacek, N. (2015). Expression of the vault RNA protects cells from undergoing apoptosis. *Nat. Commun.* 6, 7030.
- Baltz, A.G., Munschauer, M., Schwanhäusser, B., Vasile, A., Murakawa, Y., Schueler, M., Youngs, N., Penfold-Brown, D., Drew, K., Milek, M., et al. (2012). The mRNA-bound proteome and its global occupancy profile on protein-coding transcripts. *Mol. Cell* 46, 674–690.
- Beckmann, B.M., Horos, R., Fischer, B., Castello, A., Eichelbaum, K., Al-jeaume, A.M., Schwarzl, T., Cruk, T., Foehr, S., Huber, W., et al. (2015). The RNA-binding proteomes from yeast to man harbour conserved enigmRBPs. *Nat. Commun.* 6, 10127.
- Berger, W., Steiner, E., Grusch, M., Elbling, L., and Micksche, M. (2009). Vaults and the major vault protein: novel roles in signal pathway regulation and immunity. *Cell. Mol. Life Sci.* 66, 43–61.
- Bjorkoy, G., Lamark, T., Brech, A., Outzen, H., Perander, M., Overvatn, A., Stenmark, H., and Johansen, T. (2005). p62/SQSTM1 forms protein aggregates degraded by autophagy and has a protective effect on huntingtin-induced cell death. *J. Cell Biol.* 171, 603–614.
- Boersema, P.J., Rajmakers, R., Lemeer, S., Mohammed, S., and Heck, A.J. (2009). Multiplex peptide stable isotope dimethyl labeling for quantitative proteomics. *Nat. Protoc.* 4, 484–494.

Carpenter, A.E., Jones, T.R., Lamprecht, M.R., Clarke, C., Kang, I.H., Friman, O., Guertin, D.A., Chang, J.H., Lindquist, R.A., Moffat, J., et al. (2006). CellProfiler: image analysis software for identifying and quantifying cell phenotypes. *Genome Biol.* 7, R100.

Carroll, B., Otten, E.G., Manni, D., Stefanatos, R., Menzies, F.M., Smith, G.R., Jurk, D., Kenneth, N., Wilkinson, S., Passos, J.F., et al. (2018). Oxidation of SQSTM1/p62 mediates the link between redox state and protein homeostasis. *Nat. Commun.* 9, 256.

Castello, A., Horos, R., Strein, C., Fischer, B., Eichelbaum, K., Steinmetz, L.M., Krijgsveld, J., and Hentze, M.W. (2013). System-wide identification of RNA-binding proteins by interactome capture. *Nat. Protoc.* 8, 491–500.

Castello, A., Fischer, B., Frese, C.K., Horos, R., Alleaume, A.M., Foehr, S., Curk, T., Krijgsveld, J., and Hentze, M.W. (2016). Comprehensive identification of RNA-binding domains in human cells. *Mol. Cell* 63, 696–710.

Castello, A., Frese, C.K., Fischer, B., Järvelin, A.I., Horos, R., Alleaume, A.M., Foehr, S., Curk, T., Krijgsveld, J., and Hentze, M.W. (2017). Identification of RNA-binding domains of RNA-binding proteins in cultured cells on a system-wide scale with RBDmap. *Nat. Protoc.* 12, 2447–2464.

Cha-Molstad, H., Yu, J.E., Feng, Z., Lee, S.H., Kim, J.G., Yang, P., Han, B., Sung, K.W., Yoo, Y.D., Hwang, J., et al. (2017). p62/SQSTM1/Sequestosome-1 is an N-recognin of the N-end rule pathway which modulates autophagosome biogenesis. *Nat. Commun.* 8, 102.

Ciuffa, R., Lamark, T., Tarafder, A.K., Guesdon, A., Rybina, S., Hagen, W.J., Johansen, T., and Sachse, C. (2015). The selective autophagy receptor p62 forms a flexible filamentous helical scaffold. *Cell Rep.* 11, 748–758.

Donohue, E., Balgi, A.D., Komatsu, M., and Roberge, M. (2014). Induction of covalently crosslinked p62 oligomers with reduced binding to polyubiquitinated proteins by the autophagy inhibitor verteporfin. *PLoS ONE* 9, e114964.

Durán, A., Serrano, M., Leitges, M., Flores, J.M., Picard, S., Brown, J.P., Moscat, J., and Diaz-Meco, M.T. (2004). The atypical PKC-interacting protein p62 is an important mediator of RANK-activated osteoclastogenesis. *Dev. Cell* 6, 303–309.

Duran, A., Amanchy, R., Linares, J.F., Joshi, J., Abu-Baker, S., Porollo, A., Hansen, M., Moscat, J., and Diaz-Meco, M.T. (2011). p62 is a key regulator of nutrient sensing in the mTORC1 pathway. *Mol. Cell* 44, 134–146.

Frankel, L.B., Lubas, M., and Lund, A.H. (2017). Emerging connections between RNA and autophagy. *Autophagy* 13, 3–23.

Galluzzi, L., Baehrecke, E.H., Ballabio, A., Boya, P., Bravo-San Pedro, J.M., Cecconi, F., Choi, A.M., Chu, C.T., Codogno, P., Colombo, M.I., et al. (2017). Molecular definitions of autophagy and related processes. *EMBO J.* 36, 1811–1836.

Guo, H., Chitiprolu, M., Gagnon, D., Meng, L., Perez-Iratxeta, C., Lagace, D., and Gibbons, D. (2014). Autophagy supports genomic stability by degrading retrotransposon RNA. *Nat. Commun.* 5, 5276.

Hentze, M.W., Castello, A., Schwarzl, T., and Preiss, T. (2018). A brave new world of RNA-binding proteins. *Nat. Rev. Mol. Cell Biol.* 19, 327–341.

Huppertz, I., Attig, J., D'Ambrogio, A., Easton, L.E., Sibley, C.R., Sugimoto, Y., Tajnik, M., König, J., and Ule, J. (2014). iCLIP: protein-RNA interactions at nucleotide resolution. *Methods* 65, 274–287.

Hussain, S., Sajini, A.A., Blanco, S., Dietmann, S., Lombard, P., Sugimoto, Y., Paramor, M., Gleeson, J.G., Odom, D.T., Ule, J., and Frye, M. (2013). NSun2-mediated cytosine-5 methylation of vault noncoding RNA determines its processing into regulatory small RNAs. *Cell Rep.* 4, 255–261.

Itakura, E., and Mizushima, N. (2011). p62 Targeting to the autophagosome formation site requires self-oligomerization but not LC3 binding. *J. Cell Biol.* 192, 17–27.

Izquierdo, M.A., Scheffer, G.L., Flens, M.J., Giaccone, G., Broxterman, H.J., Meijer, C.J., van der Valk, P., and Scheper, R.J. (1996). Broad distribution of the multidrug resistance-related vault lung resistance protein in normal human tissues and tumors. *Am. J. Pathol.* 148, 877–887.

Jackson, W.T. (2015). Viruses and the autophagy pathway. *Virology* 479–480, 450–456.

Kato, H., Takahasi, K., and Fujita, T. (2011). RIG-I-like receptors: cytoplasmic sensors for non-self RNA. *Immunol. Rev.* 243, 91–98.

Kedersha, N.L., and Rome, L.H. (1986). Isolation and characterization of a novel ribonucleoprotein particle: large structures contain a single species of small RNA. *J. Cell Biol.* 103, 699–709.

Kickhoefer, V.A., Rajavel, K.S., Scheffer, G.L., Dalton, W.S., Scheper, R.J., and Rome, L.H. (1998). Vaults are up-regulated in multidrug-resistant cancer cell lines. *J. Biol. Chem.* 273, 8971–8974.

Klionsky, D.J., Abdelmohsen, K., Abe, A., Abedin, M.J., Abeliovich, H., Acevedo Arozena, A., Adachi, H., Adams, C.M., Adams, P.D., Adeli, K., et al. (2016). Guidelines for the use and interpretation of assays for monitoring autophagy (3rd edition). *Autophagy* 12, 1–222.

Komatsu, M., Kurokawa, H., Waguri, S., Taguchi, K., Kobayashi, A., Ichimura, Y., Sou, Y.S., Ueno, I., Sakamoto, A., Tong, K.I., et al. (2010). The selective autophagy substrate p62 activates the stress responsive transcription factor Nrf2 through inactivation of Keap1. *Nat. Cell Biol.* 12, 213–223.

Kraft, C., Deplazes, A., Sohrmann, M., and Peter, M. (2008). Mature ribosomes are selectively degraded upon starvation by an autophagy pathway requiring the Ubp3p/Bre5p ubiquitin protease. *Nat. Cell Biol.* 10, 602–610.

Lamark, T., Perander, M., Outzen, H., Kristiansen, K., Øvervatn, A., Michaelsen, E., Bjørkøy, G., and Johansen, T. (2003). Interaction codes within the family of mammalian Phox and Bem1p domain-containing proteins. *J. Biol. Chem.* 278, 34568–34581.

Li, F., Chen, Y., Zhang, Z., Ouyang, J., Wang, Y., Yan, R., Huang, S., Gao, G.F., Guo, G., and Chen, J.L. (2015). Robust expression of vault RNAs induced by influenza A virus plays a critical role in suppression of PKR-mediated innate immunity. *Nucleic Acids Res.* 43, 10321–10337.

Lim, J., Lachenmayer, M.L., Wu, S., Liu, W., Kundu, M., Wang, R., Komatsu, M., Oh, Y.J., Zhao, Y., and Yue, Z. (2015). Proteotoxic stress induces phosphorylation of p62/SQSTM1 by ULK1 to regulate selective autophagic clearance of protein aggregates. *PLoS Genet.* 11, e1004987.

Meurs, E., Chong, K., Galabru, J., Thomas, N.S., Kerr, I.M., Williams, B.R., and Hovanessian, A.G. (1990). Molecular cloning and characterization of the human double-stranded RNA-activated protein kinase induced by interferon. *Cell* 62, 379–390.

Miñones-Moyano, E., Friedländer, M.R., Pallares, J., Kagerbauer, B., Porta, S., Escaramís, G., Ferrer, I., Estivill, X., and Martí, E. (2013). Upregulation of a small vault RNA (svtRNA2-1a) is an early event in Parkinson disease and induces neuronal dysfunction. *RNA Biol.* 10, 1093–1106.

Nandy, C., Mrázek, J., Stoiber, H., Grässer, F.A., Hüttenhofer, A., and Polacek, N. (2009). Epstein-barr virus-induced expression of a novel human vault RNA. *J. Mol. Biol.* 388, 776–784.

Oriol, A., Praz, V., Lhôte, P., and Hernandez, N. (2016). Human MAF1 targets and represses active RNA polymerase III genes by preventing recruitment rather than inducing long-term transcriptional arrest. *Genome Res.* 26, 624–635.

Pankiv, S., Clausen, T.H., Lamark, T., Brech, A., Bruun, J.A., Outzen, H., Øvervatn, A., Bjørkøy, G., and Johansen, T. (2007). p62/SQSTM1 binds directly to Atg8/LC3 to facilitate degradation of ubiquitinated protein aggregates by autophagy. *J. Biol. Chem.* 282, 24131–24145.

Pantopoulos, K., and Hentze, M.W. (1995). Nitric oxide signaling to iron-regulatory protein: direct control of ferritin mRNA translation and transferrin receptor mRNA stability in transfected fibroblasts. *Proc. Natl. Acad. Sci. USA* 92, 1267–1271.

Pashev, I.G., Dimitrov, S.I., and Angelov, D. (1991). Crosslinking proteins to nucleic acids by ultraviolet laser irradiation. *Trends Biochem. Sci.* 16, 323–326.

Ran, F.A., Hsu, P.D., Wright, J., Agarwala, V., Scott, D.A., and Zhang, F. (2013). Genome engineering using the CRISPR-Cas9 system. *Nat. Protoc.* 8, 2281–2308.

Rappaport, J., Mann, M., and Ishihama, Y. (2007). Protocol for micro-purification, enrichment, pre-fractionation and storage of peptides for proteomics using StageTips. *Nat. Protoc.* 2, 1896–1906.

Sahani, M.H., Itakura, E., and Mizushima, N. (2014). Expression of the autophagy substrate SQSTM1/p62 is restored during prolonged starvation depending on transcriptional upregulation and autophagy-derived amino acids. *Autophagy* 10, 431–441.

Schneider, C.A., Rasband, W.S., and Eliceiri, K.W. (2012). NIH Image to ImageJ: 25 years of image analysis. *Nat. Methods* 9, 671–675.

Sica, V., Galluzzi, L., Bravo-San Pedro, J.M., Izzo, V., Maiuri, M.C., and Kroemer, G. (2015). Organelle-specific initiation of autophagy. *Mol. Cell* 59, 522–539.

Stadler, P.F., Chen, J.J., Hackermüller, J., Hoffmann, S., Horn, F., Khaitovich, P., Kretzschmar, A.K., Mosig, A., Prohaska, S.J., Qi, X., et al. (2009). Evolution of vault RNAs. *Mol. Biol. Evol.* 26, 1975–1991.

Suchanek, M., Radzikowska, A., and Thiele, C. (2005). Photo-leucine and photo-methionine allow identification of protein-protein interactions in living cells. *Nat. Methods* 2, 261–267.

Vasu, S.K., Kedersha, N.L., and Rome, L.H. (1993). cDNA cloning and disruption of the major vault protein alpha gene (mvpA) in Dictyostelium discoideum. *J. Biol. Chem.* 268, 15356–15360.

Wassarman, K.M., and Storz, G. (2000). 6S RNA regulates *E. coli* RNA polymerase activity. *Cell* 101, 613–623.

Wurzer, B., Zaffagnini, G., Fracchiolla, D., Turco, E., Abert, C., Romanov, J., and Martens, S. (2015). Oligomerization of p62 allows for selection of ubiquitinated cargo and isolation membrane during selective autophagy. *eLife* 4, e08941.

Yin, Z., Pascual, C., and Klionsky, D.J. (2016). Autophagy: machinery and regulation. *Microb. Cell* 3, 588–596.

Zaffagnini, G., Savova, A., Danieli, A., Romanov, J., Tremel, S., Ebner, M., Peterbauer, T., Sztacho, M., Trapanone, R., Tarafder, A.K., et al. (2018). p62 filaments capture and present ubiquitinated cargos for autophagy. *EMBO J.* 37, e98308.

Zatloukal, K., Stumptner, C., Fuchsbaichler, A., Heid, H., Schnoelzer, M., Kenner, L., Kleinert, R., Prinz, M., Aguzzi, A., and Denk, H. (2002). p62 is a common component of cytoplasmic inclusions in protein aggregation diseases. *Am. J. Pathol.* 160, 255–263.

Zheng, Y.T., Shahnazari, S., Brech, A., Lamark, T., Johansen, T., and Brumell, J.H. (2009). The adaptor protein p62/SQSTM1 targets invading bacteria to the autophagy pathway. *J. Immunol.* 183, 5909–5916.

STAR★METHODS

KEY RESOURCES TABLE

REAGENT or RESOURCE	SOURCE	IDENTIFIER
Antibodies		
Rabbit polyclonal anti-p62	MBL	Cat#:PM045
Mouse monoclonal anti-p62	NOVUS	Cat#:H00008878-M01; RRID:AB_437085
Rabbit polyclonal anti-TDP43	ProteinTech	Cat#:10782-2-AP; RRID:AB_615042
Mouse monoclonal anti-B-actin	Sigma-Aldrich	Cat#:A5441; RRID:AB_476744
Rabbit polyclonal anti-LC3B	MBL	Cat#:PM036; RRID:AB_2274121
Rabbit monoclonal anti-GABARAP	CST	Cat#:13733
Rabbit polyclonal anti-NBR1	PTG	Cat#:16004-1-AP; RRID:AB_2251178
Rabbit monoclonal anti-phospho-Ser757 ULK1	CST	Cat#:14202; RRID:AB_2665508
Rabbit monoclonal anti-ULK1	CST	Cat#:8054; RRID:AB_11178668
Rabbit polyclonal anti-phosphoThr389 S6K1	CST	Cat#:9205; RRID:AB_330944
Rabbit monoclonal anti-S6K1	CST	Cat#:2708; RRID:AB_390722
Rabbit polyclonal anti-phospho-Ser4E-BP1	CST	Cat#:9451; RRID:AB_330947
Rabbit monoclonal anti-4E-BP1	CST	Cat#:9644; RRID:AB_2097841
Mouse monoclonal anti-Ub (FK2)	Tebu-Bio	Cat#:AB120; RRID:AB_10541840
Rabbit polyclonal anti-GAPDH	Sigma-Aldrich	Cat#:G9545; RRID:AB_796208
Goat anti-mouse IgG-HRP	Santa Cruz	Cat#:Sc-2005; RRID:AB_631736
Goat anti-rabbit IgG-HRP	Santa Cruz	Cat#:Sc-2004; RRID:AB_631746
Mouse anti-LC3B	Cosmo Bio	Cat#:CTB-LC3-2-IC
Anti-mouse IgG Alexa Fluor 488	CST	Cat#:4408 AB_10694704
Anti-rabbit IgG Alexa Fluor 555	CST	Cat#:4413 AB_10694110
Bacterial and Virus Strains		
<i>E.coli</i> BL21(DE3) CodonPlus-RIL	Agilent	Cat#:230240
Chemicals, Peptides, and Recombinant Proteins		
Bafilomycin A1	InVivoGen	Cat#:tlrl-baf1
MG132	InVivoGen	Cat#:tlrl-mg132
4-thiouridine	Biomol	Cat#:T2933
DAPI	Roche	Cat#:10236276001
HSC CellMask Deep Red	Thermo Fisher	Cat#:H32721
Critical Commercial Assays		
TRI-reagent	Sigma-Aldrich	Cat#:T9424
Alt-R	IDT	N/A
Quick DNA Miniprep Kit	Zymogen	Cat#:D4074
Nucleofector 4D	Lonza	Cat#:SF
Lipofectamine 3000	Thermo Fisher	Cat#:L3000008
Lipofectamine RNAi max	Thermo Fisher	Cat#:13778075
MEGAshortscript	Thermo Fisher	Cat#:AM1354
Anti-HA magnetic beads	Thermo Fisher	Cat#:88836
Maxima RT kit	Thermo Fisher	Cat#:K1671
Deposited Data		
p62 iCLIP data	this paper	Array Express E-MTAB-4894
Experimental Models: Cell Lines		
HuH-7	Beckmann et al., 2015	N/A
HuH-7 Flp-In T-Rex	Beckmann et al., 2015	N/A

(Continued on next page)

Continued

REAGENT or RESOURCE	SOURCE	IDENTIFIER
HeLa	Castello et al., 2013	N/A
NIH 3T3	C. Merten laboratory	N/A
RAW264.7	M.Muckenthaler laboratory	N/A
Hep-56.1D	M.Muckenthaler laboratory	N/A
Hepa1-6	M.Muckenthaler laboratory	N/A
Oligonucleotides		
sgRNAs, crRNAs, PCR primers and Northern blotting probes - please refer to the Table S4	this paper	N/A
Recombinant DNA		
pcDNA5-FRT-TO-FLAG/HA-p62 wt and variants	this paper	N/A
pETM43-MBP-3C-p62-His6 wt and variants	this paper and Ciuffa et al., 2015	N/A
pUC57-T7-vtRNAs	this paper	N/A
pUC57-H1-vtRNAs	this paper	N/A
pSpCas9(BB)-2A-GFP	Ran et al., 2013	Addgene plasmid#: 48138
pSpCas9(BB)-2A-RFP/Cer3	kind gift from Noh lab, EMBL	N/A
Software and Algorithms		
Vienna fold	University of Vienna	http://rna.tbi.univie.ac.at/
iCOUNT	University of Ljubljana	https://icount.readthedocs.io/en/latest/
Prism GraphPad	GraphPad Software	Version 4
ImageJ	NIH	https://imagej.net/Welcome
CellProfiler	Carpenter et al., 2006	https://cellprofiler.org/
HuH-7 RBDmap data analysis	this paper	http://www.hentze.embl.de/public/RBDmapHuH7/vignettes/result/
p62 iCLIP data analysis	this paper	http://www.hentze.embl.de/public/p62-iCLIP

CONTACT FOR REAGENT AND RESOURCE SHARING

Further information and requests for resources and reagents should be directed to and will be fulfilled by the Lead Contact, Matthias W. Hentze (hentze@embl.de).

EXPERIMENTAL MODELS AND SUBJECT DETAILS

HuH-7 cells (human male origin) were cultured in low glucose (5mM) DMEM supplemented with 10% heat inactivated FCS (PAA), 2mM L-glutamine (25030081, Thermo Fisher) and 100 U/ml PenStrep (15140122, Thermo Fisher). We derived a HuH-7 Flp-In TREx cell line using published protocols (Flp-In T-Rex, Thermo Fisher), and prepared stably expressing doxycycline-inducible cell lines following manufacturer's instructions. Stable cell lines were grown in medium containing blasticidin (5µg/ml) and zeocin (100 µg/ml) or hygromycin (200 µg/ml). Induction was performed with doxycycline at 100 ng/ml overnight. HeLa (human female origin), Hepa1-6 (mouse origin), Hep-56.1D (mouse female origin), RAW264.7 (mouse male origin) and NIH 3T3 cells (mouse origin) were grown in high glucose DMEM supplement as above. Cell lines were not authenticated. *E.coli* BL21(DE3) CodonPlus-RIL cells were pre-cultured overnight at 37°C at 220 rpm in LB broth containing 34 µg/ml kanamycin and 34 µg/ml chloramphenicol. 25 mL of the saturated overnight culture was added to the ZY autoinduction media (LB broth without NaCl) containing 34 µg/ml kanamycin and 34 µg/ml chloramphenicol and incubated at 37°C for 6 hours with agitation at 200 rpm.

METHOD DETAILS**Transfections and treatments**

Transfections were done using Lipofectamine 3000 (L3000008, Thermo Fisher) for the plasmid DNA, or Lipofectamine RNAiMax (13778075, Thermo Fisher) for the siRNA and LNAs. Bafilomycine A₁ (t1rl-baf1, InvivoGen) was diluted in DMSO to 100 µM and used at 50-100 nM for 4-6 hours. 4-thiouridine (T2933, Biomol) was used at 100 µM for 16 hours. MG132 (t1rl-mg132) was used at 0.25µM concentration overnight. For starvation, cells were washed twice with PBS and starved in low glucose DMEM lacking amino acids (D9800-13, USBiological) and serum.

RNA interactome capture

RNA interactome capture was performed with minor modifications in the cell lysis procedure as previously described (Castello et al., 2013). Shortly, cells were washed twice with PBS on ice before UV crosslinking at 150 mJ/cm². Cells were lysed directly with lysis buffer (20 mM pH7.5 Tris HCl, 500 mM LiCl, 0.5% LiDS, 1 mM EDTA, 5 mM DTT) on the cell culture plates, scraped and lysates were sheared through a 27G needle before incubation with oligo d(T) beads (volume ratio lysate to beads 15:1) for 1 hour at 4°C. Beads were then washed twice with lysis buffer, twice with wash buffer 1 (20 mM pH7.5 Tris HCl, 500 mM LiCl, 0.1% LiDS, 1 mM EDTA, 5 mM DTT), twice with wash buffer 2 (20 mM pH7.5 Tris HCl, 500 mM LiCl, 1 mM EDTA, 5 mM DTT, 0.01% NP40) and twice with wash buffer 3 (20 mM pH7.5 Tris HCl, 200 mM LiCl, 1 mM EDTA, 5 mM DTT). RNAs were eluted using elution buffer (20 mM pH7.5 Tris HCl, 1 mM EDTA) and pooled eluates from three rounds of purification were used for RNase treatment with 10 U of RNase A and 10 U of RNase T1 for 30 min at 37°C. Samples were then concentrated using Amicon 3K columns (UFC500396, Merck Millipore) and mixed with 4x sample buffer (4xSB) (200mM Tris-HCl pH6.8; 8% SDS; 40% Glycerol, 0.04% bromophenol blue, 400mM DTT; 10% beta mercaptoethanol) before loading on SDS-PAGE.

Polynucleotide kinase (PNK) assay

The cells were washed twice with PBS on ice before UV crosslinking at 150 mJ/cm², lysed in lysis buffer (100mM NaCl; 50mM Tris-HCl pH7.5; 0.1% SDS; 1 mM MgCl₂; 0.1 mM CaCl₂; 1% NP40; 0.5% sodium deoxycholate; protease inhibitors (11873580001, Roche)) and homogenized by ultrasound (level 4, 3x 10sec, 50% amplitude) on ice. After homogenization the lysates were treated with 10 ng/μl of RNase A (R5503, Sigma-Aldrich) and 2U/ml Turbo DNase (AM2238, Thermo Fisher) for 15 min at 37°C, cooled on ice and used for IPs. For the Figure 1B, a series of RNaseA dilution was used. After the IP and 3 washes with lysis buffer, beads were washed additionally twice with PNK buffer (50mM NaCl; 50mM Tris-HCl pH7.5; 10mM MgCl₂; 0.5% NP-40; protease inhibitors (11873580001, Roche)), then resuspended in PNK buffer containing 0.1 μCi/μl [γ -32P] rATP (Hartmann), 1 U/μl T4 PNK (NEB), 1mM DTT and labeled for 15 min at 37°C. After 4 washes with PNK (without DTT) buffer, proteins were eluted at low pH (0.1M glycine pH2.0), neutralized with 0.2M Tris-HCl pH8.5, and mixed with 4xSB buffer. Samples were resolved by SDS-PAGE and blotted on nitrocellulose membrane. The membrane was exposed overnight to phosphorimager screen or to the imaging film (Z350397-50EA, Sigma), followed by western blotting.

p62 iCLIP

iCLIP was performed as published (Huppertz et al., 2014) using following IP procedure. 0.75-1.5 μg of p62 antibody or appropriate control IgG was coupled for 1 hour at RT to 12.5 μl of Protein G coupled magnetic beads (10004D, Thermo Fisher). Cells were washed twice with cold PBS, lysed in lysis buffer (100mM NaCl; 50mM Tris-HCl pH7.5; 0.1% SDS; 1 mM MgCl₂; 0.1 mM CaCl₂; 1% NP40; 0.5% sodium deoxycholate; protease inhibitors (11873580001, Roche)) and homogenized by ultrasound (level 4, 3x 10sec, 50% amplitude) on ice. Treatment of the lysates with RNasel (AM2295, Thermo Fisher) was used at 20 U/ml. Lysates containing 2 mg of total protein were used for IP for 1 hour at 4°C, washed three times with high salt buffer (500mM NaCl; 20mM HEPES pH7.3; 1% NP-40; 0.1% SDS; 1 mM EDTA; 0.5% sodium deoxycholate; protease inhibitors (11873580001, Roche)) and three times with the lysis buffer. Next, beads were incubated for 16 h (1 100 rpm, 16°C) in 20 μL ligation mix (50 mM Tris-HCl pH 7.5, 10 mM MgCl₂, 10 mM DTT, 500 U/ml T4 RNA ligase 1, 500 U/ml RNasin, 1.5 μM preadenylated linker L3 [5'-rApp-AGATCGGAA GAGCGGTTCAAG-ddC-3'], 20% PEG-400 [Sigma]) and washed three times with lysis buffer. Complexes were eluted at low pH (0.1M glycine pH2.0), neutralized with 1M Tris-HCl pH8.5, digested with proteinase K and used for all subsequent steps as described previously (Huppertz et al., 2014). cDNA libraries obtained after PCR amplification with universal Solexa primers (25 cycles) were multiplexed and sequenced using an Illumina HiSeq2000 platform.

Native p62 IP and protein-protein co-IP

Cells were washed twice with PBS on ice. For co-IP variant, cells were treated with 0.5mM DSP (Thermo Fisher #22585) for 1h and quenched with Tris-HCl as recommended by vendor. Cells were lysed directly on the plates with lysis buffer (20mM Tris HCl pH7.4, 100mM NaCl; 1mM EDTA; 1mM EGTA; 1% Triton X-100; protease inhibitors (11873580001, Roche); 5 μg/ml RNAsin (Promega)) by swelling 5min on ice, followed by scraping. Lysates were homogenized by pipetting against the plate and 5sec vortex. Lysates were centrifuged for 10 min at 11,800xg at 4°C and supernatant was used for IP. IP was performed either using p62 antibodies (as above) or 25 μl HA-beads slurry (Pierce). Lysis buffer washes were applied 6x and tubes were renewed after every second wash. Proteins were eluted as described above and analyzed with western blotting. Alternatively, eluates were directly resuspended in TRI reagent (T9424, Sigma-Aldrich) and RNA was purified according to manufacturer's protocol. 5μg of linear acrylamide (Thermo, AM9520) was used as carrier and RNA was resuspended in 10 μl water.

qRT-PCR

0.5 μg of total RNA or 7 μl of IP RNA was used for cDNA synthesis using Maxima RT kit (Thermo Fisher, K1671). Typically, 5ng of cDNA was used for qPCR. Primers are listed in Table S4.

RNA isolation and Northern blotting

RNA was isolated using TRI reagent (T9424, Sigma-Aldrich) as recommended by the manufacturer. RNA was dissolved in nuclease-free water and stored at -80°C . Typically, 10 or 15 μg of total RNA was mixed with 2x loading dye (95% formamide; 0.025% xylene cyanol and bromophenol blue; 18mM EDTA; 0.025% SDS), denatured for 5 min at 95°C , cooled on ice and loaded on 8% acrylamide (19:1), 7M urea polyacrylamide gels. A semi-dry blotting apparatus was used for blotting on Hybond N⁺ membranes (RPN1520B, GE) which were UV auto-crosslinked, pre-hybridized for 1 hour at 50°C and used for hybridizations with ^{32}P labeled DNA antisense oligonucleotide probes (Table S4) overnight at 50°C . The membranes were then washed three times with high stringency buffer (5X SSC; 5% SDS), three times with low stringency buffer (1X SSC; 1% SDS) and exposed to phosphorimaging screens for 4 hours or overnight. Screens were scanned at Typhoon FLA-7000 (GE) and TIFF images were quantified by ImageJ.

RBDmap

Shortly, HuH-7 lysates and oligo-d(T) captures were done as for the RNA interactome capture method. After washes and elution (eluate 1), 3 μg of LysC was added to the eluate 1 and incubated at 37°C for 8h. Afterward, aliquots for protein and RNA quality controls were harvested. Next, second oligo-d(T) capture was applied on the LysC-treated eluate 1, while the flow-through after oligo-d(T) incubation was saved. Washes were applied and elution (eluate 2) was applied. Next, inputs, eluates and flow-through were used for RNase treatment with 10 U of RNase A and 10 U of RNase T1 for 30 min at 37°C . Proteomics analysis was performed and analyzed as described (Castello et al., 2016). Shortly, cysteines were reduced (5 mM DTT, 56°C , 30 min) and alkylated (10 mM Iodoacetamide, 30 min in the dark). Samples were buffer-exchanged into 50 mM triethylammoniumbicarbonate, pH 8.5, using 3 kDa centrifugal filters (Millipore, UFC500396) and digested with sequencing grade trypsin (Promega, V5280; enzyme-protein ratio 1:50) at 37°C for 18 h. Resulting peptides were desalted and labeled using stable isotope reductive methylation (Boersema et al., 2009) on StageTips (Rappsilber et al., 2007). Labels were swapped between replicates. Labeled samples were combined and fractionated into 12 fractions on an 3100 OFFGEL Fractionator (Agilent) using Immobiline DryStrips (pH 3-11 10 NL, 13 cm; GE Healthcare) according to the manufacturer's protocol. Isoelectric focusing was carried out at a constant current of 50 mA allowing a maximum voltage of 8000 V. When 20 kWh were reached the fractionation was stopped, fractions were collected and desalted using StageTips. Samples were dried in a vacuum concentrator and reconstituted in MS loading buffer (5% DMSO 1% formic acid). Samples were analyzed on a LTQ-Orbitrap Velos Pro mass spectrometer (Thermo Scientific) coupled to a nanoAcquity UPLC system (Waters). Peptides were loaded onto a trapping column (nanoAcquity Symmetry C18, 5 μm , 180 $\mu\text{m} \times 20$ mm) at a flow rate of 15 $\mu\text{l}/\text{min}$ with solvent A (0.1% formic acid). Peptides were separated over an analytical column (nanoAcquity BEH C18, 1.7 μm , 75 $\mu\text{m} \times 200$ mm) using a 110 min linear gradient from 7%–40% solvent B (acetonitrile, 0.1% formic acid) at a constant flow rate of 0.3 $\mu\text{l}/\text{min}$. Peptides were introduced into the mass spectrometer using a Pico-Tip Emitter (360 μm outer diameter \times 20 μm inner diameter, 10 μm tip, New Objective). MS survey scans were acquired from 300–1700 m/z at a nominal resolution of 30000. The 15 most abundant peptides were isolated within a 2 Da window and subjected to MS/MS sequencing using collision-induced dissociation in the ion trap (activation time 10 msec, normalized collision energy 40%). Only 2+/3+ charged ions were included for analysis. Precursors were dynamically excluded for 30 s (exclusion list size was set to 500). The RBDmap dataset and analysis can be accessed at <http://www.hentze.embl.de/public/RBDmapHuH7/vignettes/result/>.

Protein extracts, SDS-PAGE and western blotting

For western blotting, cells were washed twice with ice cold PBS on ice and lysed on plate using RIPA lysis buffer (89900, Thermo Fisher) supplemented with protease inhibitor (11873580001, Roche). Lysates were treated with benzonase (100U/ml, 71206, Merck Millipore) for 15 min on ice and protein concentrations were measured. Lysates were mixed with 4xSB, boiled for 5 min and typically 15 μg of lysate was used for SDS-PAGE. Proteins were transferred to nitrocellulose or PVDF membranes using the Trans-Blot Turbo Transfer System (Bio-Rad) and blocked for 1 hour at room temperature with 5% milk in PBS; 0,05% Tween (PBS-T). Primary antibodies were incubated in 5% milk PBS-T either overnight at 4°C or 1 hour at RT, followed by 3x PBS-T washes, secondary antibody incubation in 5% milk in PBS-T for 1 hour at RT, 3x PBS-T washes and developed using ECL (WBKLS0500, Millipore). Primary and secondary antibodies used for western blotting are listed in the [Key Resources Table](#).

siRNA, LNAs

An siRNA pool targeting p62 (L-010230-00-0020, GE) was used at 30 nM concentration for 48 hours. As control siRNA an equimolar mix of Scramble (5' UUCUCCGAACGUGUCACGUtt 3'; s229174, Thermo Fisher), sLuciferase (5' CGGAUUACCAGGGAUUCAtt 3'; Thermo Fisher) and SWNeg9 (5' UACGACCGGUCUAUCGUAGtt 3'; s444246, Thermo Fisher) was used. LNAs (Exiqon) targeting vtRNA1-1 (#1: 5' ttaaagaactgtcgaa 3'; #3: 5'ttaaagaactgtcga 3') and control negA (5' aacacgtctatacgc 3') were used at 25 or 50 nM for 48 hours.

Cloning

Full length human p62 WT cDNA was cloned into pcDNA5_FRT/TO vector with N-terminal FLAG/HA tag (MDYKDDDDKSAGGY PYDVPDYAKL...) using HindIII and Xhol sites. Single and double amino acid mutations were done using PCR-mediated mutagenesis. Recognition sites of p62 siRNA were mutated in synonymous fashion (5' GGATCGAGGTAGACATAGA 3'; 5' GAGCAAATG GAATCCGACA 3'; 5' GGACGCACCTCTCATCTAA 3'; 5' CGACTGGCCTCAAAGAGGC 3'), cDNA was synthetized in pUC57

(GenScript) and swapped into p62 cDNA using BamHI and Xhol sites. Vault RNA with T7 or H1(2xTO) promoters were synthetized (GenScript) in pUC57 backbone.

CRISPR/Cas9 gene deletion of vtRNA1-1

Single guide RNAs targeting the *vtRNA1-1* locus (Table S4) were predicted using the CRISPR online tool (<http://crispor.tefor.net>; Version May 2017) (Ran et al., 2013), ordered from Sigma-Aldrich, annealed and cloned into pSpCas9(BB)-2A-GFP (PX458) (Addgene plasmid #48138 kindly provided by Fang Zhang), pSpCas9(BB)-2A-RFP or pSpCas9(BB)-2A-Cer3 (both kindly provided by Kyung-Min Noh, EMBL) using the BbsI restriction sites. Different combinations of the generated plasmids (see Figure S6B) were nucleofected into HuH-7 cells using the Nucleofector 4D system according to manufacturer's guidelines (Lonza, Cell Line Nucleofector Kit SF, program FF137, 1 million cells and 1 µg of DNA per nucleofection). As negative control a mixture of all parental plasmids (without sgRNA) was used. Single cell sort of double/triple positive cells was performed 48h after nucleofection. Upon clone expansion the genomic DNA was isolated (Zymo, Quick-DNA Miniprep Kit) and a PCR was performed to screen for homozygous deletions of the vault RNA1-1 (see Table S4 for primers, Figure S6C). Resulting vaultRNA1-1 KO clones were further validated by qPCR (Figure S6D). In order to detect possible off-target effects all vault RNA paralogs were included into the screen.

CRISPR/Cas9 mediated p62 gene inactivation

Alt-R kit (IDT) was used for p62 gene inactivation. In short, HuH-7 cells were transfected with 3nM RNP complexes using 2 different crRNAs (Table S4) and cell sorted 48 hours later using tracRNA-Atto 550nm. Single cell derived clones were grown out and analyzed by western blotting. Positive clones were cultured in the presence of 100nM BafA for 5 hours and re-analyzed by western blotting using 2 different p62 antibodies (Figure S5B). Genomic locus spanning p62 ATG was amplified for selected clones (primers sequences in Table S4), cloned into TA plasmid (Thermo Fisher, K204001) and sequenced. For all experiments presented in the main Figures p62KO clone I-E7 was used.

In vitro transcription and EMSA

pUC57 plasmid with T7_vault RNA1-1 was used for *in vitro* transcription reaction using MEGAshortscript kit (AM1354, Thermo Fisher) with ^{32}P - α UTP (SRP-210, Hartmann) according to the manufacturer's protocol. RNA was gel purified, phenol-chloroform extracted, dissolved in water and measured for the specific activity with scintillation counter and concentration with QuBit (Thermo). Before the reaction, RNA was denatured 10 min at 65°C and cooled down to room temperature. Afterward MgCl₂ was added to 2.5mM. IRE RNA element production was described (Pantopoulos and Hentze, 1995). EMSA reaction contained typically 0.025-6 µM of proteins, 15 nM of RNA (150 fmol, 3-5kCPM), 1 mg/ml of BSA, 10 µg/µl RNasin, 5mM DTT, 0.5mM PMSF, 2.5mM MgCl₂, 100mM KCl; 20mM HEPES pH7.9; 0.2 mM EDTA and 20%glycerol. Reactions were incubated 20 min at room temperature. After the reaction samples were loaded on 20cm long 5% acrylamide native gel and ran overnight at 70V. Gel was dried for 1 hour at 80°C and exposed 4h or overnight to phosphorimager screen.

p62 protein expression and purification

MBP-p62-his₆ was expressed in *E.coli* BL21(DE3) CodonPlus-RIL cells by autoinduction in ZY media. After pre-culture at 37°C for 6 hours, cell cultures were cooled down to room temperature and incubated for 16 hr at 20°C. Cells were lysed by resuspension in lysis buffer (50mM HEPES pH 8.0, 1M NaCl, 0.5 mM TCEP, 1x protease inhibitor) followed by four passes through a microfluidizer. Lysate was clarified by centrifugation at 48 000xg and incubated with Ni-NTA beads for 1 hr. Beads were washed extensively in buffer 1 (50mM HEPES pH 8.0, 1M NaCl, 0.5 mM TCEP, 50mM Imidazole) and protein eluted with buffer 2 (50mM HEPES pH 8.0, 1M NaCl, 0.5 mM TCEP, 250mM Imidazole).

Immunofluorescence microscopy and image analysis

For immunostaining, cells were cultured on ibidi slides (80426; ibidi), fixed for 10 min with methanol, washed with PBS, permeabilized and blocked for 1 hour in 0.1% Triton X-100 in 1% BSA solution. Cells were then incubated with primary antibodies for 1 hour at room temperature, washed in PBS and incubated with the secondary antibody, DAPI and Cell Mask for 1 h at room temperature in the dark. Slides were washed 3 times in PBS and stored at 4°C in PBS until imaging. Reagents used were anti-p62 (1:1000, #PM045, MBL), anti-LC3B (1:200; #CTB-LC3-2-IC, Cosmo Bio), anti-mouse IgG Alexa Fluor 488 (1:1000; #4408, Cell Signaling), anti-Rabbit IgG Alexa Fluor 555 (1:1000; #4413, Cell Signaling), DAPI (#10236276001, Roche); HSC CellMask Deep Red stain (1:40 000; #H32721, Thermo Fisher). Images of the fluorescent staining were acquired on a Leica SP5 confocal microscope using a 63x/NA1.2 PlanApo water immersion lens. Excitation and emission settings were as follows: Dapi (Ex 405nm / Em 410 - 484 nm), Alexa Fluor 488 (Ex 488nm / Em 500 – 551 nm) and Alexa Fluor 555 (Ex 561 nm / Em 564 – 628 nm), and Cell Mask Deep Red (Ex 633 nm / Em 661 – 714 nm). One image dataset comprised one z stack with 24 slices acquired at 335 nm spacing, each slice consisting of 1024 × 1024 pixels with a pixel size of 120 nm x 120 nm. Typically, 10 such image datasets were acquired per condition and replicate. For visual inspection and quantitative single cell analysis in CellProfiler 2.2.0 (Carpenter et al., 2006) z-maximum projections were computed using ImageJ (Schneider et al., 2012). Using CellProfiler, nuclei were segmented in the DAPI channel by means of an intensity threshold. Cells were segmented by an image-based watershed algorithm, computed on the Cell Mask Deep Red staining, using segmented nuclei as seeds. LC3 and p62 objects were segmented in the respective antibody

staining images by applying a morphological tophat filter for enhancement of locally bright structures followed by an intensity threshold. LC3 and p62 objects were counted as co-localizing if the pixel based overlap was greater than or equal to three pixels. To ensure an unbiased analysis all settings of the analysis pipeline such as all intensity thresholds and filter settings were kept unchanged across all conditions and replicates.

Chemical synthesis of XIE62-1004-A

XIE62-1004-A (2-((3,4-bis(benzyloxy)benzyl)amino)ethan-1-ol) was chemically synthesized starting from 3,4-dihydroxybenzaldehyde according to the literature procedure described by [Cha-Molstad et al. \(2017\)](#) with the following modifications. The crude 2-((3,4-bis(benzyloxy)benzyl)amino)ethan-1-ol was purified by silica gel column chromatography using a NH3(aq.)/MeOH/CH2Cl2 mixture for elution (1/1/98 → 1/10/89). The product obtained as colorless oil was re-dissolved in HPLC grade CHCl3, aliquoted into eppendorf tubes and then the solvent was evaporated in a Speedvac overnight. XIE62-1004-A was used as a 500 mM DMSO stock.

QUANTIFICATION AND STATISTICAL ANALYSIS

Data are displayed as single points, mean ± SEM; Student's t test was used, *n* values are indicated in the respective Figure legends. *p*-values are indicated in the Figures, *p* < 0.05 was considered statistically significant. GraphPad Prism v4.0 was used to create plots. Images were quantified with ImageJ.

DATA AND SOFTWARE AVAILABILITY

The sequencing data was deposited to Array Express with the accession number E-MTAB-4894: <https://www.ebi.ac.uk/arrayexpress/experiments/E-MTAB-4894/?page=1&pagesize=500>

The analysis of the p62 iCLIP datasets is described at <http://www.hentze.embl.de/public/p62-iCLIP>. RNA secondary structures were predicted using the ViennaRNA package.

Supplemental Figures

Cell

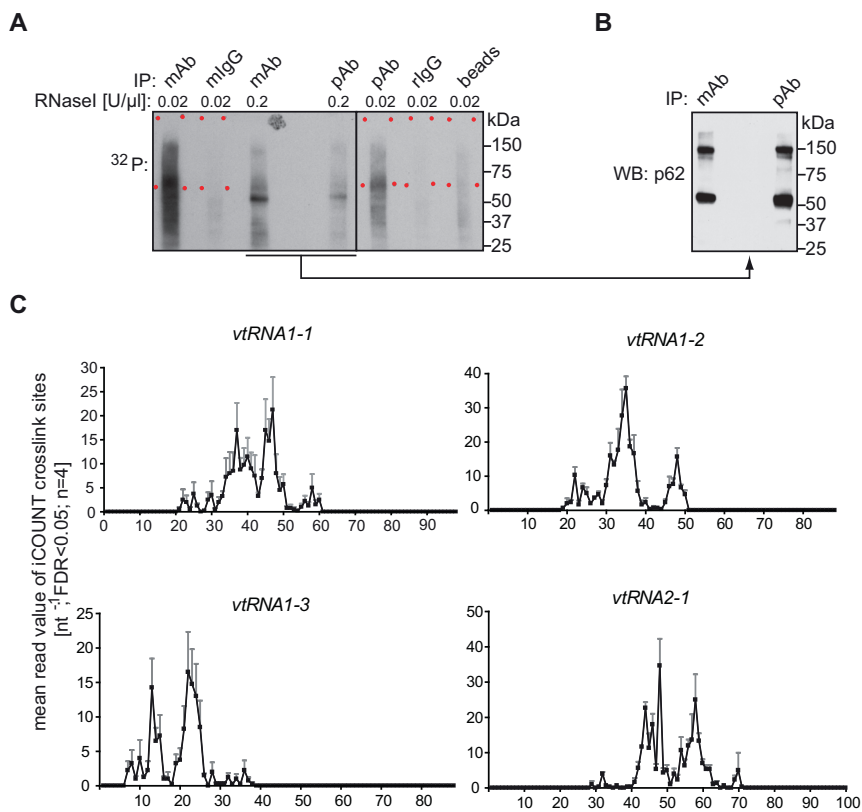


Figure S1. iCLIP Analysis of p62, Related to Figure 1

(A) Lysates from 254nm UV-C light exposed HuH-7 cells were treated with a low (20U/ml RNase I, L) or high concentration of RNase I (200 U/ml, H), and used for IPs with the indicated antibodies and controls. p62-RNA complexes were separated by SDS-PAGE, blotted and excised as indicated by the red dotted rectangles. The underlined area of the blot was used for a subsequent western blotting shown in panel (B). (C) p62 crosslink site (CS) analysis on vtRNAs. Significant (FDR 5%) CS read counts of p62 IPs displayed on the vtRNAs transcript sequence.

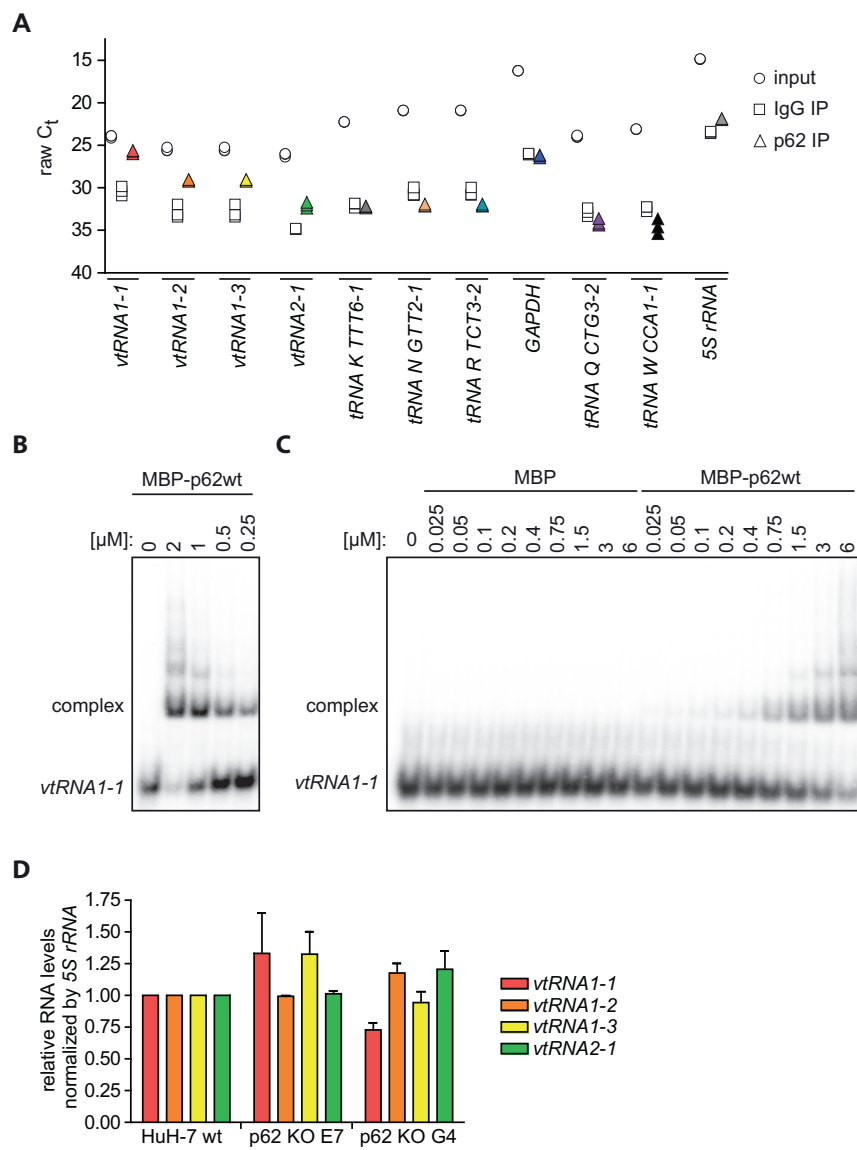


Figure S2. *In Cellulo* and *In Vitro* p62-vtRNA1-1 Analysis, Related to Figure 2

(A) Raw RT-qPCR Ct values related to Figure 2A. (B) EMSA using MBP-p62 and radiolabeled vtRNA1-1. (C) Representative EMSA using MBP-p62 and radio-labeled vtRNA1-1, with unlabeled non-specific competitor RNA included. (D) qRT-PCR analysis of total RNA from wt or p62 KO HuH-7 cells; $n = 3$.

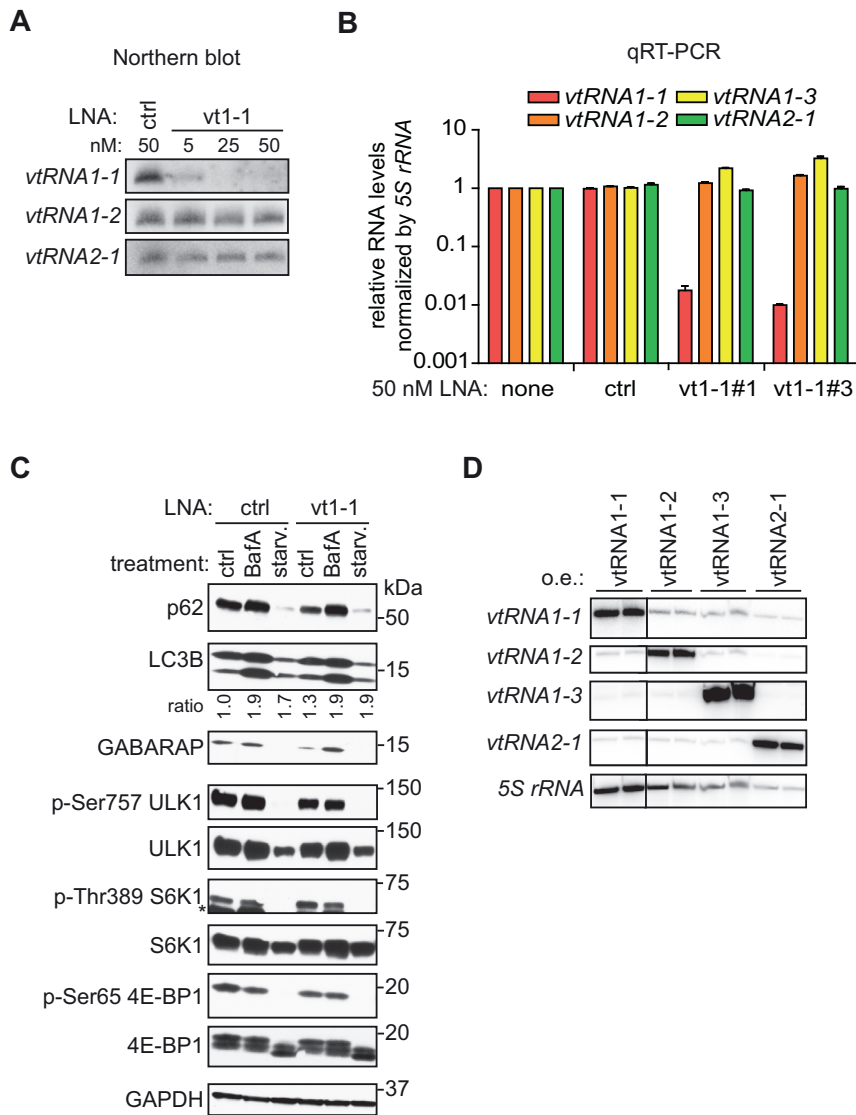


Figure S3. *vtRNA1-1* Phenotypic Analysis, Related to Figure 3

(A,B) Cells were transfected with indicated amounts of LNA and lysed after 48 hours. Total RNA was isolated and analyzed by Northern blotting (A), representative image, and by qRT-PCR (B); n = 3. (C) Cells were transfected with control LNA or LNA targeting *vtRNA1-1* and incubated for 48 hours. Cells were then subjected to following treatments: control, 100 nM BafA for 5h, or media lacking amino acids (-AA) for 4h. Lysates were analyzed by western blotting. * indicates a non-specific band. (D) Cells were transfected with the indicated expression vectors, total RNA was extracted after 24h and analyzed by Northern blotting.

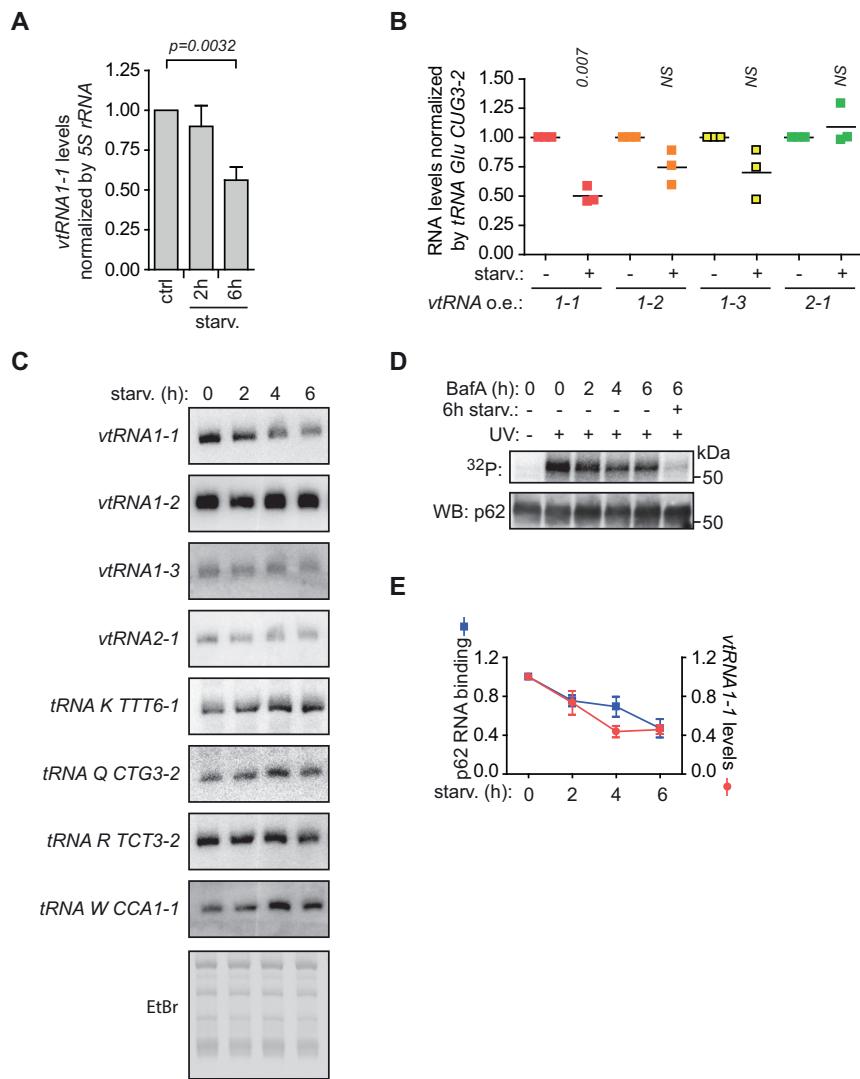


Figure S4. Starvation-Mediated Regulation of vtRNA1-1 Levels, Related to Figure 4

(A) Cells were treated as indicated and used for total RNA isolation and analysis by qRT-PCR. n = 9 (B) Cells were transfected with the indicated expression vectors ('vtRNA o.e.'), and 24 hours later were either starved for 6h or control treated. Total RNA was extracted and analyzed by Northern blotting. Probe signals were quantified and plotted as data relative to non-starved control. n = 3 (C) Cells were starved for the indicated times, total RNA was extracted, and analyzed by Northern blotting with indicated probes. (D) Cells were starved in minimal medium containing solvent control or BafA at 100 nM for the indicated time, 254nm UV-C light exposed and lysed. Lysates were used for p62 IPs and RNA radiolabeling assay. After SDS-PAGE and transfer, the membrane was exposed overnight on film and used subsequently for western blotting. (E) Data of quantified RNA-bound p62/total p62 from Figure 4C is plotted together with the total vtRNA1-1 levels acquired from the HuH-7 cells starved in minimal media for indicated time and measured by Northern blotting; n = 3

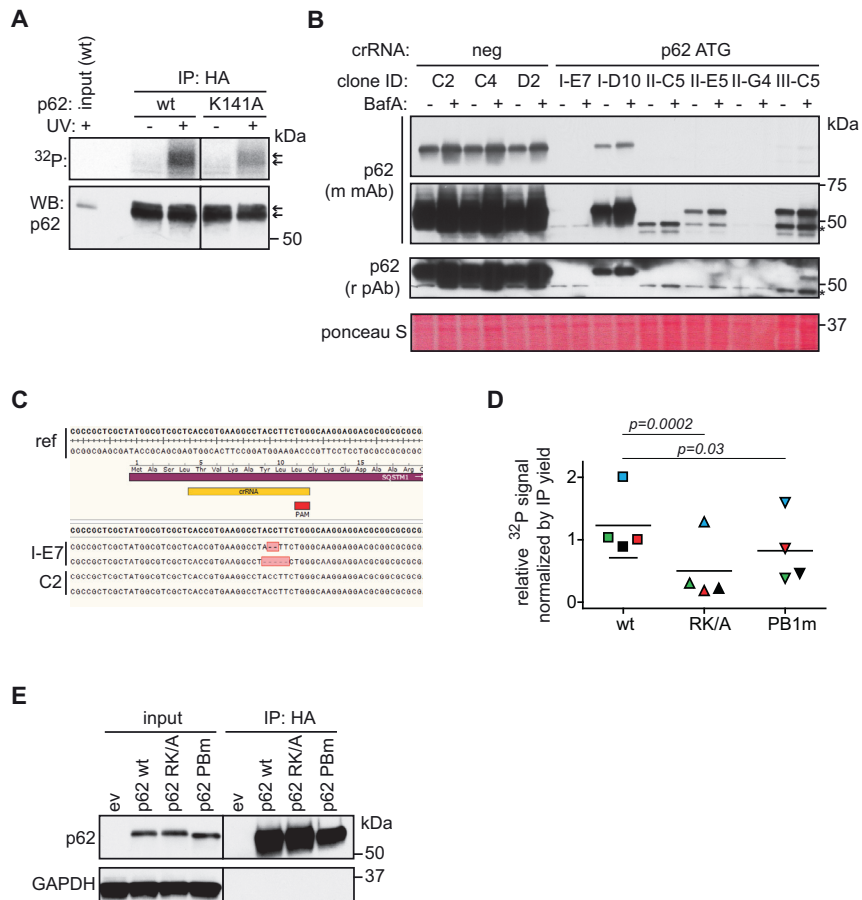


Figure S5. p62 PNK Analysis and HuH-7 p62KO Cell Generation, Related to Figure 5

(A) HuH-7 wt cells stably expressing tagged p62 wt or K141A variant subjected to UV-C 254nm, lysed and used for HA IP followed by RNA radiolabeling assay. Arrows indicate the endogenous (lower band) and exogenous (upper band) p62, respectively. (B) Western blotting analysis of stable HuH-7 p62 KO CRISPR clones analyzed for the expression of p62. * indicates a non-specific band. (C) Sanger sequencing analysis of the p62 genomic locus around ATG. Reference genomic sequence ("ref") is displayed on the top. Two lines for each clone represent alleles identified in the TA cloning for the amplified PCR fragment. (D) Quantification of radiolabeling experiments related to Figure 5D. The colors indicate paired replicates. (E) Representative western blot analysis of HA IP eluates related to Figure 5E.

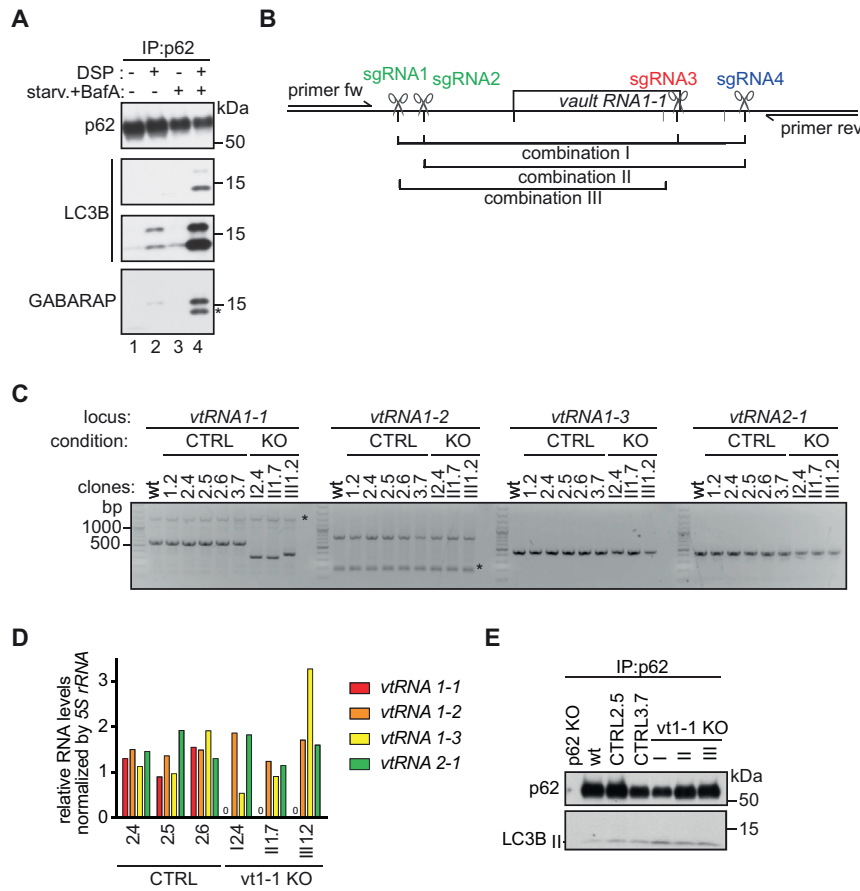


Figure S6. p62 CoIP Analysis and HuH-7 vtRNA1-1 KO Cells Generation, Related to Figure 6

(A) HuH-7 cells were treated as indicated (starv.+BafA indicates 5h in starvation media in the presence of 100 nM BafA). Cells were then crosslinked using DSP, lysed and used for p62 IPs. Eluates were analyzed by SDS-PAGE and visualized by western blotting. * indicates band from previous LC3B antibody stain (B) Schematic representation of the genomic locus of *vtRNA1-1*. Localization of guide RNAs and primers for PCR analysis are indicated. The combinations of guide RNAs for CRISPR are shown. (C) PCR analysis of genomic loci of the respective vault RNAs for wt, control and CRISPR KO clones. * indicates a non-specific amplicon. (D) qRT-PCR analysis of vault RNAs from total RNA of selected CRISPR clones. "0" indicates no value detected. (E) Western blotting analysis of p62 co-IP eluates. IP from lysates of indicated cell clones cultured in the presence of BafA for 5h at 100 nM and treated with DSP.